U.S. DEPARTMENT OF ENERGY | Office of Science

ARM-97-003

Science and Experiment Plan
Fall 1997 Flight Series

R Ellingson
T Tooman

Fall 1997

ARM
CLIMATE RESEARCH FACILITY

Exploratory Systems Technologies
Sandia National Laboratories
7011 East Avenue
Livermore, California 94551-0969

ARM – UAV

Atmospheric Radiation Measurement – Unmanned Aerospace Vehicle

Science and Experiment Plan

Fall 1997 Flight Series

Robert Ellingson and Tim Tooman, eds.

Version 2.1 July 14, 1997

Table of Contents

Introduction

Objectives

The ARM-UAV (Atmospheric Radiation Measurement - Unmanned Aerospace Vehicle) Program is a multi-agency, multi-laboratory program funded by the Department of Energy. The program uses a variant of a UAV originally developed for defense surveillance as a remotely piloted platform for making important climate measurements. Using a UAV to make these measurements offers the significant advantage of high-altitude and long-endurance operations, two features that are very important when studying evolving cloud fields and their effect on the solar and thermal radiation balance in the atmosphere, a major goal of the ARM-UAV program. Additionally, the program is seeking to exploit the high altitude flight capability of UAVs to provide measurements to calibrate satellite radiance products and validate their associated flux retrieval algorithms.

A corollary to these scientific goals is the technical objective of using improved measurement techniques and instruments for radiative fluxes, cloud properties, and *in situ* water vapor that were developed earlier in this program. The demonstration of this objective was begun in the four previous flight campaigns flown in the spring of 1994, fall of 1995, spring of 1996, and fall of 1996 and will be continued in the fall 1997 campaign discussed herein.

Science Questions

As with the ARM program the primary scientific focus of the ARM-UAV program is on radiation-cloud interactions. Uncertainties in how clouds interact with the earth s solar and thermal radiation account for almost the entire factor of three variation in the predicted temperature rise for a doubling of atmospheric CO_2. While some of these uncertainties can be addressed by the ground-based measurements being made in the ARM program, others require measurements from within the atmosphere. For example, the measurement of atmospheric heating in a slab requires the measurement of the net fluxes at the top and bottom of the slab as well as the relevant cloud properties and water vapor profiles. Satellite based measurements are a natural way of extending these process measurements to larger scales but would benefit from the additional calibration and validation that carefully controlled high altitude aircraft measurements can provide.

Previous experiments, most notably the ARM-UAV fall 1995 campaign known as ARESE and the Spring 1996 and the Fall 1996 campaigns have suggested that cloudy skies absorb more shortwave radiation than predicted by current models. Unfortunately, instrumentation, flight opportunities, and meteorological conditions did not permit the acquisition of an unchallengeable data set in this regard on previous flights. Therefore, shortwave absorption questions continue to dominate the science issues for this fall 1997 campaign. There is also a set of issues to be explored in this campaign related to the characterization of surface optical properties that could refine the surface parameters required by relevant models to predict radiation-cloud interactions.

Approach

As noted above, the approach is to use UAVs because of their promise for sustained endurance at altitudes up to 20 km. However, in this campaign, we will use an Altus UAV that has only a single stage of turbocharging, and whose ceiling is thus limited to 13.7 km. A chase aircraft supports the Altus during low altitude operations and serves as a second, low level instrumented platform when the Altus is at altitude.

An ARM-UAV Science Team has provided guidance for the preparation of this science plan, and its members are responsible for the usage and analysis of data from all UAV instrumentation. Team members are identified in the descriptions of the various experiments.

Campaign History and Resources

During the initial phases of the ARM-UAV program, spanning the three year period between late calendar 1993 and late 1996 four aircraft were flown in four separate campaigns with payloads comprised of a subset of nineteen different instruments. The aircraft and their planned payload complements are discussed below. All four campaigns were flown at the Southern Great Plains (SGP) Cloud and Radiation Testbed (CART) Site in north central Oklahoma in the spring of 1994, fall of 1995, spring of 1996, and fall of 1996.

The first campaign used the General Atomics Gnat 750, a midsize UAV capable of carrying a 100-kg payload to a maximum altitude of 7 km. The Gnat was first operated in a checkout flight at Edwards Air Force Base with a basic radiometric payload in November, 1993, and again at the SGP CART site in April, 1994, for a seven flight science mission, called UDF. The operable payload contained four broadband radiometers plus a downwelling TDDR developed by Francisco Valero   the radiometers were the four combinations of upwelling and downwelling, solar and thermal. Valero, Gore, and Giver, 1982; Valero, Ackerman, and Gore, 1989; and Valero and Pilewskie, 1992 describe these instruments. Additionally the payload included an *in situ* package with total temperature, pressure, and dew point sensors. There are no plans to fly this UAV in conjunction with the experiments discussed in this science plan.

The General Atomics Altus, capable of carrying a 150-kg payload to a 10-km altitude, was utilized in the fall 1996 campaigns. Its payload included the Gnat 750 instruments (with a frost point hygrometer instead of the dew point sensor) plus a SSP, CDL, and MPIR. These latter instruments are described below.

A DHC-6 Twin Otter manned aircraft was flown during all campaigns as a chase plane for the various UAVs and as a low level instrumented platform in all but UDF. Its instrument suite includes four Valero radiometers covering various broad spectral bands for both upwelling and downwelling fluxes, two TDDRs for upwelling and downwelling spectral fluxes, and an *in situ* package with total temperature, total pressure, differential pressure, and dew point sensors. In the two 1996 campaigns the Otter also carried a microwave radiometer to determine total cloud water and columnar water vapor.

A Grob Egrett manned aircraft, capable of carrying a 200-kg payload to greater than 16-km altitude, was flown in the fall 1995 and spring 1996 campaigns. Its instrument suite is the same as that mentioned for the Altus UAV.

In the current campaign, the Altus and DHC-6 Otter will again be flown. Both aircraft will carry the same payloads as in the fall of 1996, with slight modifications to the Frost Point Hygrometer and the Microwave Radiometer. Although the MPIR and CDL can each be mounted in the Altus payload, weight and volume limitations may require either the MPIR or CDL be off loaded for any given flight.

New Instrument Developments

Seven new UAV compatible instruments have been developed by or for the ARM-UAV program. Since these are not well documented in open literature they will be discussed briefly here, except for the *in situ* frost point hygrometer, which is a natural extension of the well known dew point hygrometers. This new hygrometer was first flown on the third campaign.

The Cloud Detection LIDAR, or CDL, was developed by LLNL based on technology from the Clementine moon mapping mission for the profiling of aerosols, profiling of optically thin clouds, and determining cloud top or base height of optically thick clouds. It features a fully eyesafe 100 μJ/pulse 5 kHz laser with a divergence of 53 μrad and a wavelength of 1.05 μm. The receiver telescope has a 20 cm aperture. The entire system can be rotated in flight for either nadir or zenith viewing, and has a coaxial CCD camera to image the cloud fields. The CDL was first flown on the second campaign.

The UAV Atmospheric Emitted Radiance Interferometer (UAV AERI) is being developed at the University of Wisconsin as a derivative of the ground-based AERI based at the SGP cart site. It has approximately 0.5 cm^{-1} spectral resolution across 3-25 μm spectral coverage band. Its viewing mirror can be rotated in flight to study either upwelling or downwelling radiation with a spatial resolution of 1-10 km. This instrument has an on board calibration source. The UAV AERI will not be flown before 1998.

The Hemispherical Optimized Net Radiometer, or HONER, detects the net difference between upwelling and downwelling fluxes to about 3% accuracy. It has greater than 170° FOV upward and downward and covers the 0.3 to 4 μm shortwave and 4 to 50 μm longwave bands. The HONER will not be flown before 1998, but will be tested at an earlier date on a ground-based stand.

The Multispectral Pushbroom Imaging Radiometer, or MPIR, uses filtered linear detector arrays for nine band coverage of upwelling radiation. The arrays have 256 elements, with a total cross track FOV of ±40° and in track direct nadir FOV of 6 mrad. The nine bands are 0.62-0.67, 0.86-0.90, 1.36-1.39, 1.58-1.64, 2.11-2.22, 3.55-3.93, 6.54-6.99, 8.40-8.70, and 10.30-11.30 μm. These were chosen with cloud water and water vapor studies in mind. Images from the arrays are captured twice per second, so the aircraft s velocity relative to the imaged scene determines in track image. MPIR was first flown on the third campaign. Only the four shortest wavelength bands will be available for the fall 1997 campaign.

A UAV compatible variant of the Solar Spectral Flux Radiometer, SPFR, was to be flown on the Altus for the first time in the fifth or fall 1997 campaign, but its development was not completed in time for payload integration. It will thus be flown first in the spring or summer 1998 campaign. The SPFR covers a 300 nm - 2500 nm spectral range with 5-10 nm resolution while operating in one of two modes: irradiance (hemispheric) or radiance (narrow field of view 1 mrad). Both modes have zenith and nadir pointing optic heads. Several parameters may be retrieved from the data taken by the SPFR, including cloud water phase, optical depth, particles size, liquid/ice water path, and liquid/ice water content.

A microwave radiometer MWR system consisting of 22 and 37 GHz channels is flown in an upward viewing mode on the DHC-6. The 22/37 MWR system has been previously flown as part of the Airborne Multichannel Microwave Radiometer, AMMR, on the NASA DC-8 aircraft, and was first flown in the ARM-UAV program in the third campaign. A new 22/37 and 89 GHz MWR system is being constructed specifically for the DOE ARM-UAV program DHC-6 aircraft, but will not be flown before 1998.

Finally, a 95 GHz radar, developed at the NASA Goddard Space Flight Center for operation on the NASA ER-2 aircraft is being modified for ground based operation during the ARM-UAV autumn campaign. The modifications include construction of a mounting that permits elevation angle scanning, a large aperture antenna (1 m, 57-dBi gain), and the development of a data logging system.

While the technology is not unique to the ARM-UAV program, the INS/GPS system flown on all the aircraft described above is crucial to the success of experiments involving two stacked aircraft. It allows pilots, whether in the aircraft or in a UAV ground control station, to control the lateral separation of their platforms to within several hundred meters. Additionally, the attitude sensing function of this system provides critical information for the reduction of radiometric data with a direct solar component.

Document Structure

The bulk of this document describes four experiments that have been proposed for the next campaign. Since most of these require specific meteorological conditions, the experiment suite for this fall 1997 campaign will be a subset of these, with the details of the subset depending on the conditions encountered during the course of the campaign. The appendices provide contact information and a glossary of acronyms.

Experiment Group 1 Geostationary Satellite over the SGP Central Facility

Part A Science Issues

Science Objective

The objectives are (i) to characterize the radiation budget of the atmospheric column above the CART site extending from the surface to the UAV flight altitude on onward to the TOA in cloudy and aerosol laden clear conditions, (ii) to characterize the radiative properties of clouds within that same column, (iii) to relate these properties to measurements of broadband fluxes at the surface and flight altitudes, and (iv) to determine as accurately as possible the microphysical properties of the clouds that are used to compute cloudy sky absorption.

The radiative heating of the atmosphere induced by clouds is an important component of the energy budget of the atmosphere. The relationship between this heating and the (optical) properties of clouds and aerosols is not well developed for the following reasons. (i) Accurate measurements of the column heating have been elusive in the past, and have been affected by 3D structure of clouds and biases introduced by inadequate sampling and limitations of experimental design. (ii) Characterizing the full 3D properties of clouds, notably their relevant optical properties, has also proved elusive at best, especially in the case of aircraft-based field programs.

This ARM-UAV experiment proposes to overcome these problems as much as possible by maintaining the UAV above the central facility in mode that will effectively enable the UAV to hover above the surface sensors, thereby providing maximum overlap not only between surface and aircraft observations, but also between aircraft and satellite measurements. This is desirable since the surface cloud profiling sensors (millimeter wave radar and lidar) are crucial for characterizing the cloud and its structure. The sensors on the UAV, such as the CDL, SSP, and MPIR together with additional measurements from the surface sensors, will provide the best possible estimate of the cloud or aerosol optical properties. These in turn can be compared to similar properties derived from satellite radiances and to similar properties deduced from the surface instruments. Deployment of in *situ* aircraft is desirable to assist in the validation of the derived cloud or aerosol properties.

A particularly bothersome problem has been the interpretation of the altitude dependence of radiative measurements over clouds. Data gathered simultaneous at two levels above a cloud deck could be used to estimate the spectral smoothing scale of the cloud. This result will provide an empirical measure of the amount of spatial smoothing required to infer broadband absorption from collocated flights above and below a cloud.

Cloud microphysics as quantified by phase, optical depth, particle size and shape, and cloud liquid or ice water path, determine the amount of radiation absorbed and reflected by a given cloud. The vertical and horizontal distributions of the water mass also affect the flux fields. Previous calculations of cloud absorption, used to deduce enhanced shortwave absorption from flux measurements, have assumed values for the cloud microphysical properties using one parameter such as optical depth to normalize the theoretical results to the observations. Because the other parameters also affect the reflection and absorption, the fluxes computed with the assumed values may be incorrect. By more realistically specifying the microphysical parameters in the models, the impact of this potential error source will be minimized.

Advocate

This experimental group will be conducted under the auspices of the Instantaneous Radiative Flux Working Group and the Cloud Properties Working Group. Individuals expecting to analyze the data include Catherine Gautier and (to be supplied). Additionally, Pat Minnis, Tom Ackerman, Qiang Fu, and Yefim Kogan will analyze cloud microphysical data.

Measurement Strategy

The experimental strategy, as stated above, is to optimize coordination between the Altus UAV and the surface sensors at the CART Central Facility. The principal Altus payload will include spectral (SSP, MPIR) and broadband radiometers (RAMS) and possibly the CDL. The desire is to make continuous measurements using the Altus as a quasi-stationary measuring platform at altitude above the central facility. The strategy is to: (i) measure the broadband fluxes and spectral radiances at the surface and at one or two altitudes above the central facility, (ii) obtain cloud structure information from surface remote sensors such as the MMR, (iii) obtain *in situ* measurements of cloud microphysical and thermodynamic properties that will aid in validation of cloud property estimates, and (iv) obtain *in situ* measurements of aerosol properties.

The desired flight path consists of two legs crossing over the central facility tower, oriented generally in the solar plane and perpendicular to it. The aircraft are to fly straight and level on each leg for an average of five minutes. Legs are to be flown in a fashion that alternates direction of flight for subsequent passes. When both the Altus and DHC-6 are flying, they are to maintain stations above and below each other with 4-km tolerance, and to attempt central facility over flight with less than 1-km tolerance. At some time during a flight with both aircraft, they should perform an intercomparison maneuver, i.e., one complete circuit in reasonably close formation at a convenient co-altitude.

Variant A Column to Troposphere

This variant focuses on the radiation budget of the column between the surface and the Altus. The DHC-6 is not required. Desired meteorological conditions are either aerosol laden clear or single layer, single phase, extensive cloud decks at any altitude. The Altus is ideally to fly at either its service ceiling in clear conditions or an altitude above the clouds equal to the distance between the cloud base and the surface. Measurements should start as soon after sunrise as possible and extend to as close to sunset as possible.

Variant B Aircraft Atop Clouds

This variant focuses on the smoothing of the radiation field over clouds. Both the Altus and the DHC-6 are required. Desired meteorological conditions are single layer (possibly scattered to broken), non-convective, single phase, extensive cloud. The DHC-6 is to fly near the cloud tops and the Altus at its maximum altitude. Alternatively, the Altus could fly at two or three equally spaced altitudes over the DHC-6. Measurements should be made at low SZA to minimize variation in solar angles during collection.

Variant C Aircraft Over and Under Clouds

This variant focuses on horizontal variations in cloud properties and radiation fluxes. Both the Altus and the DHC-6 are required. Desired meteorological conditions are single layer (possibly scattered to broken), non-convective, single phase, extensive cloud decks. The DHC-6 is to fly 1 to 2 km below the cloud base and the Altus a similar distance above the cloud tops. Measurements should be made at low SZA to minimize variation in solar angles during collection.

Variant D Cloud Microphysics

This variant is similar in flight strategy to variant A, but focuses on the relationship between cloud microphysics and absorption. The DHC-6 is not required, but aircraft *in situ* sampling is. Desired meteorological conditions are single layer, single phase, extensive cloud decks at any altitude. The Altus can either fly at its service ceiling or at altitudes required by variant A. Measurements should start as soon after sunrise as possible and extend to as close to sunset as possible.

Ideally, the distribution of the microphysics throughout the entire cloud field should be specified at a high resolution. Measurement of such distributions, however, is far from possible. To approximate the ideal observational system, the experiment strategy relies on a multi-platform approach. Passive remote sensors can provide a horizontal, large-scale characterization of the cloud field's bulk microphysics. Active sensors like cloud radar are used to obtain detailed information about the vertical distribution of cloud mass along a horizontal slice of the cloud field. *In situ* measurements will provide cloud "truth" for both the passive and active remote sensing systems. A combination of the various datasets will yield the most accurate depiction of the microphysics for the entire cloud field. The resulting datasets can then be used in either plane-parallel or more complex 2-D and 3-D models to compute the broadband and spectral fluxes exiting the bottom and top of the clouds for comparison with the Altus measurements.

The MPIR on the Altus will take data simultaneously with the RAMS to provide relatively high-resolution retrievals (~100 m for low clouds) of optical depth from the 0.65-μm channel, particle size from the 1.64 or 2.1-μm channels, and liquid water path from a combination of the two other retrievals. If the clouds are at high altitudes, then phase will be determined also, but the resolution will be finer because of the close proximity to cloud top. The MPIR will cover a swath maximum of ~23 km at 14 km altitude, whereas the signal from the RAMS will come from a larger area due to its hemispherical field of view. Thus, cloud properties will be needed for a larger area. Infrared (11 um) and solar infrared (3.9-um) data from GOES-8 taken at 4-km resolution every 15 min will provide the greater spatial coverage of particle size. Higher resolution, 1-km GOES-8 visible (0.65-um) data will be analyzed to provide optical depths at a better resolution. When available, data from the NOAA-12 and 14 AVHRR will be used to retrieve all of the bulk microphysical properties twice per day. These will be matched with the flight patterns of the aircraft. The microwave radiometer at the SGP Central Facility will provide an independent measure of cloud liquid water path. These data do not yield the coverage obtained with the MPIR and satellite, but can provide a means for determining the uncertainty in the other retrievals. Similarly, the surface measurements taken by the MSRFR can be used to assess the optical depths.

The cloud radar data will be analyzed to derive optical depth and vertical profiles of cloud particle size and liquid water content, which can be integrated to obtain effective radius and LWP, respectively. The results can be compared to the passive retrievals and possibly provide a basis for adjusting their derived fields. Additionally, the profiles can be used as a basis for taking the 2-D fields from the satellite and MPIR data and converting them to 3-D quantities for use in 3-D RTMs. *In situ* data taken by the non-UAV aircraft will be used to verify both the radar- and passively derived cloud properties whenever they are available.

Required and Supporting Measurements

UAV

The UAV will measure upwelling and downwelling solar fluxes in the upper troposphere with a RAMS, and upwelling spectrally resolved broadband fluxes and radiances directly below the UAV with a nadir SSP The MPIR will collect cloud image data in bands centered on 0.65, 0.88, 1.37, and 1.61 μm. The MPIR s cross track FOV will be ±40°. A desired supporting instrument is the CDL to determine distance to and variability of the cloud top altitude.

Instrumented Chase

The DHC-6 will measure upwelling and downwelling solar fluxes for Variants B and C with a RAMS, and downwelling spectrally resolved broadband fluxes and radiances directly above the DHC-6 with a zenith SSP. The MWR will measure cloud liquid water above flight altitude as a supporting measurement for variant C.

In Situ Aircraft

(To be supplied)

Ground

The GRAMS, MFRSR, and SIRS at the SGP central facility will make both broadband and spectrally resolved flux measurements. Atmospheric state properties and cloud drift due to wind will be obtained from measurements by radiosondes, the 915 MHz profiler with RASS, and the 50 MHz profiler with RASS. Water vapor and aerosol loading in the lower troposphere will be assessed using the Raman LIDAR. Cloud base will be determined using a Vaisala ceilometers (models CT25K and CT75K) and a MMCR, the latter also being important for 3D mapping of cloud extents and DD or ID. Cloud homogeneity will also be assessed using the WSI. Column LW path will be measured with a MWR. Several ground-based instruments are to be deployed for the fall SGP IOPs that will provide critical data for this group of experiments. These include (to be supplied).

Satellite

The primary instrument is the imager on GOES-8 for measurement of narrowband radiances in the visible and infrared bands. Secondarily, narrowband data will be used from the AVHRR on NOAA-12, and NOAA-14, whenever their views match the area of operations.

Data Analysis Strategy

Variant A Column to Troposphere

The data taken for this variant will supplement data for the ARESE re-reprise experiment discussed elsewhere in this experiment plan, with the substitution of ground data for that acquired by the DHC-6. The data analysis strategy is therefore a derivative of the ARESE strategy.

Three strategies will be used for evaluating cloudy or aerosol laden atmospheric absorption relative to models. These can be variously adapted to use data from the three levels of this variant s measurements: (1) surface, (2) UAV, and (3) TOA (satellite).

A direct way of evaluating cloudy sky or aerosol laden atmospheric shortwave absorption, relative to that for pristine clear skies, is to compare cloud radiative forcing at the surface to that at the TOA; that is, the difference between all-sky and clear sky net downward shortwave radiation. Models typically give a value near one for the ratio of cloud radiative forcing at the surface to cloud radiative forcing at the TOA although some recent measurements indicate a value near 1.5 might be more appropriate. Since model simulations of cloud radiative forcing are easily performed for the Altus UAV altitudes, this approach can be used to compare measurements taken on board this platform with model results.

During this experiment variant upwelling surface shortwave flux will not be measured with the same instruments used on board the aircraft since the GRAMS used on the surface has no nadir viewing components. A second analysis strategy overcomes this deficiency by substituting surface insolation for the surface net flux used in the above strategy. Models typically give a value near 1.25 for the ratio of surface cloud insolation forcing to TOA cloud radiative forcing, compared to some recent measurements indicating a value nearer 1.75 for this same ratio.

The ratio of cloud radiative forcing at the surface to that at the TOA can be shown to be mathematically equal to $-(\Delta\alpha/\Delta T)^{-1}$ where α is the TOA albedo and T is the atmospheric transmittance. This leads to a third approach that evaluates $\Delta\alpha/\Delta T$ from a linear regression of the measured quantities of albedo and transmittance. Since this approach does not require clear sky identification, it serves to remove cloud shortwave absorption from broken cloud effects.

Variant B Aircraft Atop Clouds

Because the lower aircraft cannot instantly, or fully sample, the field observed by the higher aircraft, the data analysis will tend to emphasize a statistical approach. One important statistical quantity is the spatial power spectrum (SPS) determined from the Fourier transform of the observed fluxes as a function of distance (flight time). This quantity is a powerful tool for revealing the presence (or absence) of characteristic scale lengths in the observed field. In addition, by comparing the power spectrum from various sub-samples of the data one should be able to get a measure of the adequacy of the sampling. The SPS also indicates how the variance changes with resolution.

The flights closest to the clouds will have the highest spatial resolution, and so will yield SPSs extending to the highest spatial frequency and thus give the most detailed information on characteristic scale length. These low altitude SPSs will be compared against the high altitude SPSs to verify current understanding of the effects of areal averaging on the observed fluxes. These comparisons will be done in two ways. The first will simply convolve the low altitude SPS with the field of view response function of the high altitude radiometers and compare this to the high altitude SPS. The second approach will construct models of fractal cloud fields with properties similar to the low altitude SPS and use Monte Carlo calculations to predict the observed fluxes at high altitudes.

Such analyses can be applied not only to the broadband fluxes from the SBBRs, but also to the spectrally resolved fluxes from the TDDRs with possibly different results for conservative and non-conservative scattering channels due to the dependence of photon path length on absorptivity.

Variant C Aircraft Over and Under Clouds

The main idea is to derive areal mean flux quantities and relate these to areal mean cloud properties as derived from profiles from active probes. For example, the along track flight data together with matched cloud profile data offer a unique data set to test 3D radiative transfer. Relation of cloud structure to satellite image data also offers the possibility to relate this transfer to the broader setting as seen by satellites.

The analysis strategy delineated below is suitable for the ideal case of a single cloud over the SGP central facility. Extensibility to multi-cloud situations will be addressed by modeling.

Since data collection legs begin and end far from the central cloud, the radiation fields observed at these extrema are not unduly influenced by the cloud. As the aircraft approach the cloud the scattered radiation, i.e., cloud reflectance and leakage, will cause increases in upwelling radiation on the nadir viewing radiometer on the UAV and similar increases in downwelling radiation on the zenith radiometer on the DHC-6 until shadowing or near-shadowing conditions exist. By using a convolution of (1) the nadir radiometer on the DHC-6 for accounting for surface reflectance and lower atmospheric absorption and scattering, (2) the zenith radiometer on the UAV for determining the atmospheric absorption and scattering above the cloud, and (3) a clear sky radiative transfer model tuned to these measurements to account for the absorption and scattering of radiation between the aircraft, it should be possible to derive the influence of clouds on the vertical heating profile as a function of the horizontal distance from the cloud.

These measurements provide a direct measure of the effects of clouds on the heating profile for cloudy atmospheric columns, which will be usable in climate modeling studies. These measurements will also provide a means for understanding the directional dependence of the radiation stream from clouds. Clouds are not isotropic scatterers and thus it is difficult to measure or model the directional component of scattered radiation. However, it is clearly a much more simple problem to model the radiation field for an isotropic scattering cloud, and thus it should be possible to compute what the aircraft measurements should be if the cloud were isotropic. By comparing the slopes of the simulated measurements for the isolated cloud and the actual data from the aircraft flights it may be possible to infer the directional component of the radiation scattered by the cloud. Clearly, radiance data provided by the mpir for a few viewing angles will be of help in this.

Simulations using a 3d Monte Carlo radiative transfer model are possible and could be used to determine the magnitude of radiation field disturbances expected for the proposed flight legs for this experiment as a function of a few cloud types and a few solar zenith angles.

Variant D Cloud Microphysics

Data taken for this variant from the cloud radar will be used to normalize MPIR and satellite retrievals of cloud microphysical properties and to produce a vertical structure for the horizontal cloud fields. Averages from flight data segments of approximately 15 minutes will be used for this normalization. Surface observations will be used to evaluate optical depths and LW path; *in situ* data will provide verification of particle size.

Relation to Other Experiments

As mentioned above, variant A is closely associated with the ARESE family of experiments. Variants B and C are derivatives of experiments 5 and 4, respectively, of the ARM UAV Science and Experiment Plan, 1996 Flight Series, Revision 4, March 2, 1996. Variant D is similar to experiments 7 and 9 from that same document. All variants in this group are closely linked to Shortwave, Aerosol, and Cloud Radar IOPs that are occurring concurrently with this UAV IOP at the SGP CART Site in September and October of 1997.

Part B Experiment Details

Flight Strategy

A cross pattern will be flown repetitively by the Altus and, when required, the DHC-6. One pass through the cross is shown in Figure 1. The flight sequence involves data runs in a particular order, for example from A1 to A2, A3 to A4, A2 to A1, and finally A4 to A3. Thus, each leg of the cross is flown twice, once in each direction. The legs are 24 km long, requiring 5 minutes for the Altus to traverse at altitude in wind free conditions. One iteration of the entire pattern is therefore 40 minutes, again without a wind at flight altitude.

The first leg is aligned with the sun to within ±22.5°. For series of end points are provided such that one series will always afford the needed alignment; for example, for a flight at dawn the first point of the first leg would be B3 and for one at solar noon it would be B1. As long flight progresses, the start points for successive iterations of the cross pattern are updated for the changing solar position.

Variant A Column to Troposphere

This variant requires Altus only flights from near sunrise to near sunset over single layer, single phase, extensive cloud decks. The Altus is to fly at an altitude above the clouds equal to the distance between the cloud base and the surface. This could be any altitude between the minimum for flight without escort of 18 kft (~5.5 km) and its service ceiling for this campaign of ~13.7 km. Therefore, the cloud deck tops for this variant must be between 3.2 and 7.3 km assuming a nominally thickness of 1 km.

Variant B Aircraft Atop Clouds

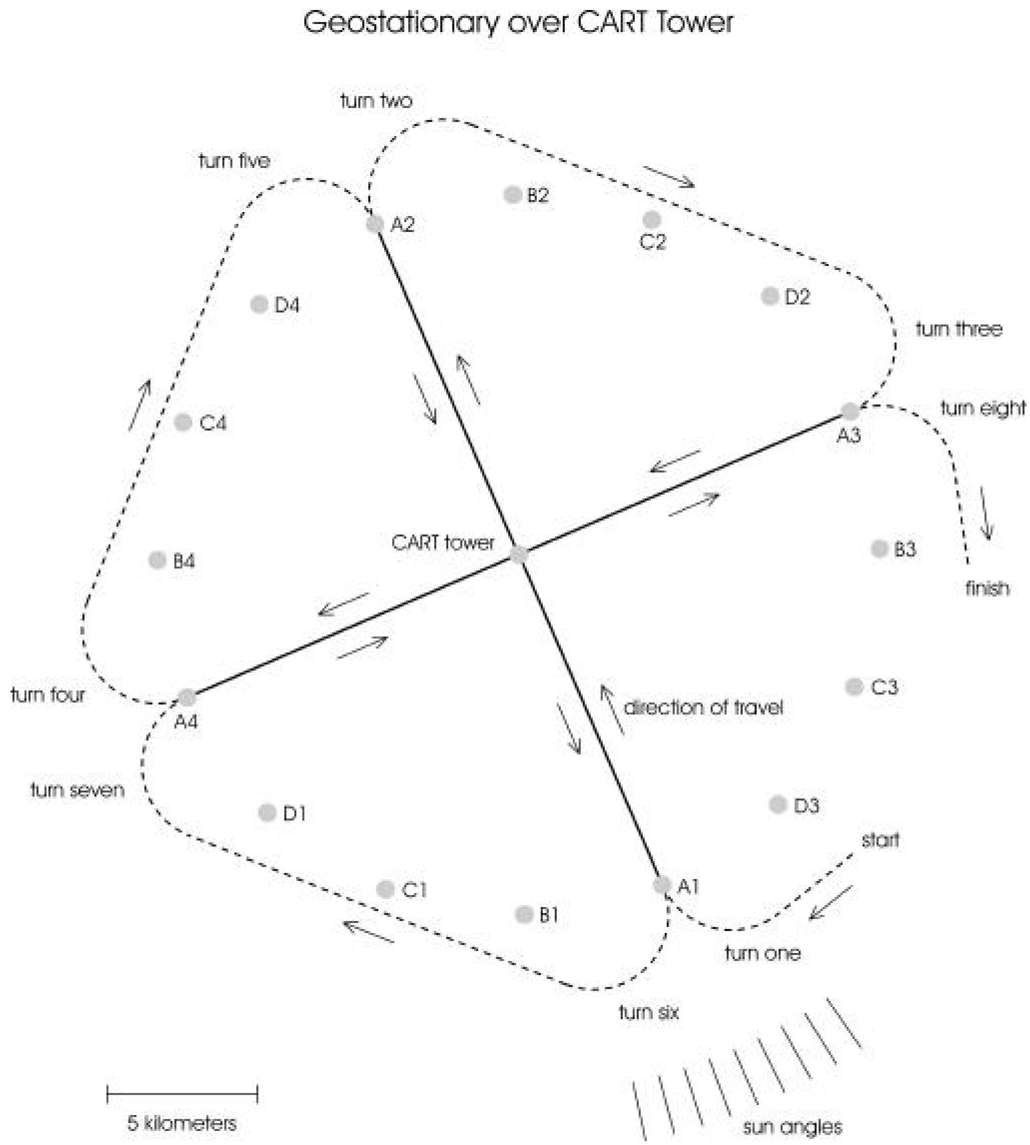

Figure 1. Flight path for Altus of DHC-6 over the SGP CART Central Facility

This variant focuses on the smoothing of the radiation field over clouds. Both the Altus and the DHC-6 are required to fly over single layer (possibly scattered to broken), non-convective, single phase, extensive cloud decks. Their flight paths are to be synchronized so that they fly over the central facility nearly simultaneously on each data leg. The DHC-6 is to fly near the cloud tops and the Altus at its maximum altitude. Since the DHC-6 operation ceiling is 20 kft (~6 km), cloud tops can be no higher than ~5.5 km. Alternatively the

Altus could fly at two or three equally spaced altitudes over the DHC-6. Measurements should be made near solar noon.

Variant C Aircraft Over and Under Clouds

As in variant B, both the Altus and the DHC-6 are required, and must fly so as to cross the central facility simultaneously on each data leg. Desired meteorological conditions are single layer (possibly scattered to broken), non-convective, single phase, extensive cloud decks. The DHC-6 is to fly 1 to 2 km below the cloud base and the Altus a similar distance above the cloud tops. Given aircraft performance limitations, useful cloud decks can have tops no lower than 3.5 km (Altus minimum non-escorted flight level is 5.5 km) and no higher that 12.7 km (Altus service ceiling is ~13.7 km). Similarly bases can be no higher than 8 km (DHC-6 service ceiling is ~6 km) and no lower that 2 km to allow penetration space beneath. Measurements should be made near solar noon.

Variant D Cloud Microphysics

Like variant A, this variant requires Altus only flights from near sunrise to near sunset over single layer, single phase, extensive cloud decks. The Altus is to fly ideally at its service ceiling of ~13.7 km but can also be deployed at an altitude above the clouds equal to the distance between the cloud base and the surface to match variant A flights.

Constraints

The following table specifies the coordinates of the four turn points for each of the four orientation sets indicated in the figure above.

Table 1. Flight Path Definition for Geostationary Satellite Pattern

Turn Point	*UTM*			*Lat*	*Long*
A1	639766	4041236	14	36°30.4' N	97°26.4' W
A2	630232	406326	14	36°42.4'	97°32.5'

		2		N	W
A3	646012	4057016	14	36°38.9'N	97°22.0'W
A4	623986	4047482	14	36°33.9'N	97°36.9'W
B1	635188	4040250	14	36°29.9'N	97°29.4'W
B2	634810	4064248	14	36°42.9'N	97°29.4'W
B3	646998	4052438	14	36°36.4'N	97°21.4'W
B4	623000	4052060	14	36°36.4'N	97°37.5'W
C1	630582	4041091	14	36°30.4'N	97°32.5'W
C2	639416	4063407	14	36°42.4'N	97°26.3'W
C3	646157	4047832	14	36°33.9'N	97°22.0'W
C4	623841	4056666	14	36°38.9'N	97°36.9'W
D1	626649	4043631	14	36°31.8'N	97°35.1'W
D2	643349	4060867	14	36°41.0'N	97°23.7'W
D3	643617	4043899	14	36°31.8'N	97°23.7'W
D4	626381	4060599	14	36°41.0'N	97°35.1'W

Special Needs

The MPIR will be in a straight nadir mount on the Altus.

Instrument and Data List

UAV

Instrument 1: MPIR (all variants) four channels (0.62-0.67 μm, 0.86-0.90 μm, 1.36-1.39 μm, and 1.58-1.64 μm) each yielding data from a 256 element linear array (512 element for band 1) that is oriented to provide a curved, across track radiometric line image; the line images are spatially co-registered and temporally sampled each 0.5 second (0.25 for band 1); the instantaneous FOV for each pixel is 6 mrad (3 mrad for band 1)

Instrument 2: nadir SSP2 (all variants) reflected spectral radiance in $Wm^{-2}sr^{-1}nm^{-1}$, 0.4 to 4.0 μm; reflected spectral flux in $Wm^{-2}nm^{-1}$, 0.4 to 2.5 μm; 2 channels linearly polarized ($||$, $\perp$) reflected spectral radiance in $Wm^{-2}sr^{-1}nm^{-1}$, 0.4 to 2.5 μm; reflected broadband radiance in $Wm^{-2}sr^{-1}$, 0.4 to 4.0 μm; reflected broadband flux in Wm^{-2}, 0.4 to 2.5 μm

Instrument 3: zenith TDDR (all variants) downwelling hemispherical flux data; seven channels each 10 nm wide; channel center wavelengths are 0.5, 0.86, 1.0, 1.25, 1.5, 1.65, and 1.75 μm; shadow rings move across the FOV periodically blocking direct solar radiation thus enabling determination of the diffuse : direct ratio

Instrument 4: nadir TDDR (all variants) upwelling hemispherical flux data; seven channels each 10 nm wide; channel center wavelengths are 0.5, 0.86, 1.0, 1.25, 1.5, 1.65, and 1.75 μm

Instrument 5: zenith FSBBR (all variants) broadband radiometer with hemispherical FOV; measures downwelling flux from 0.7 to 3 μm

Instrument 6: nadir FSBBR (all variants) broadband radiometer with hemispherical FOV; measures upwelling flux from 0.7 to 3 μm

Instrument 7: zenith SBBR (all variants) broadband radiometer with hemispherical FOV; measures downwelling flux from 0.3 to 4 μm

Instrument 8: nadir SBBR (all variants) broadband radiometer with hemispherical FOV; measures upwelling flux from 0.3 to 4 μm

Instrument 9: CDL (all variants)   200 range bins with intensity of reflected laser light plus one background bin; range bins provide information on the location and density of aerosols and clouds; background bin for data correction

Instrumented Chase

Instrument 1: MWR (variant C)   two channels at 22 and 37 GHz providing information on columnar cloud water and total liquid water along a zenith viewing path

Instrument 2: SSP1 (nadir for variant B and zenith for variant C) reflected spectral radiance in $Wm^{-2}sr^{-1}nm^{-1}$, 0.4 to 4.0 μm; reflected spectral flux in $Wm^{-2}nm^{-1}$, 0.4 to 2.5 μm; 2 channels linearly polarized ($||$, $\perp$) reflected spectral radiance in $Wm^{-2}sr^{-1}nm^{-1}$, 0.4 to 2.5 μm

Instrument 3: zenith TDDR (variants B and C)   downwelling hemispherical flux data; seven channels each 10 nm wide; channel center wavelengths are 0.5, 0.86, 1.0, 1.25, 1.5, 1.65, and 1.75 μm; shadow rings move across the FOV periodically blocking direct solar radiation thus enabling determination of the diffuse : direct ratio

Instrument 4: nadir TDDR (variants B and C)   upwelling hemispherical flux data; seven channels each 10 nm wide; channel center wavelengths are 0.5, 0.86, 1.0, 1.25, 1.5, 1.65, and 1.75 μm

Instrument 5: zenith FSBBR (variants B and C)   broadband radiometer with hemispherical FOV; measures downwelling flux from 0.7 to 3 μm

Instrument 6: nadir FSBBR (variants B and C)   broadband radiometer with hemispherical FOV; measures upwelling flux from 0.7 to 3 μm

Instrument 7: zenith SBBR (variants B and C)   broadband radiometer with hemispherical FOV; measures downwelling flux from 0.3 to 4 μm

Instrument 8: nadir SBBR (variants B and C)   broadband radiometer with hemispherical FOV; measures upwelling flux from 0.3 to 4 μm

In Situ Aircraft

(To be supplied)

Ground

Instrument 1: Raman LIDAR (variants A and D) 355 nm laser system providing profiles of water vapor, aerosols, and optically thin clouds with 40 meter resolution; maximum altitude for water vapor is 4 km daytime and 10 km night time; maximum altitude for aerosols and clouds is 15 km

Instrument 2: radiosonde (all variants) balloon borne instrument measuring temperature, pressure, water vapor, and winds from its surface launch point upwards to a 35 km altitude during a 2 hour period

Instrument 3: MMCR (all variants) zenith-pointing radar that operates at a frequency of 35 GHz to determine cloud boundaries (e.g., cloud bottoms and tops) and radar reflectivity (dBZ) of the atmosphere up to 20 km; has a Doppler capability that will allow the measurement of cloud constituent vertical velocities

Instrument 4: 915 MHz profiler with RASS (all variants) profiles of virtual temperature, wind speed, and wind direction

Instrument 5: 50 MHz profiler with RASS (all variants) profiles of virtual temperature, wind speed, and wind direction

Instrument 6: MWR (all variants) water vapor density profile and five-minute averages of column integrated water vapor, column integrated liquid water, and blackbody equivalent brightness temperature

Instrument 7: Lamont SIRS (variants A, C, and D) direct beam normal solar irradiance; downwelling diffuse solar irradiance; downwelling hemispherical solar irradiance; upwelling hemispherical solar irradiance; downwelling hemispherical infrared radiance

Instrument 8: Lamont MFRSR (variants A, C, and D) hemispheric downward solar irradiance (415, 500, 610, 665, 862, and 940 nm); hemispherical downward total solar irradiance; diffuse hemispherical downward solar irradiance (415, 500, 610, 665, 862, and 940 nm) diffuse hemispherical downward total solar irradiance; direct beam normal solar irradiance (415, 500, 610, 665, 862, and 940 nm); and direct beam normal total solar irradiance

Instrument 9: Vaisala ceilometer model CT25K (variants A, C, and D) measures cloud base height at up to three levels with a maximum vertical range of 25,000 ft (7.5 km) and a vertical resolution of about 15 m

Instrument 10: Vaisala ceilometer model CT75K (variants A, C, and D) measures cloud base height at up to three levels with a maximum vertical range of 75,000 ft (22.5 km) and a vertical resolution of about 30 m

Instrument 11: WSI (variants A, C, and D) image of entire sky dome; 0.33° angular resolution; 16 bit dynamic range; image grab every 10 sec; day time image is red filtered (650 nm) and blue filtered (450 nm); night time image not filtered; derived products include calibrated radiance map of sky dome, cloud cover fraction, and segmented image into opaque clouds, thin clouds, and clear

Instrument 12: Lamont GRAMS TDDR (variants A, C, and D) downwelling hemispherical flux data; seven channels each 10 nm wide; channel center wavelengths are 0.5, 0.86, 1.0, 1.25, 1.5, 1.65, and 1.75 μm; shadow rings move across the FOV periodically blocking direct solar radiation thus enabling determination of the diffuse: direct ratio

Instrument 13: Lamont GRAMS FSBBR (variants A, C, and D) broadband radiometer with hemispherical FOV; measures downwelling flux from 0.7 to 3 μm

Instrument 14: Lamont GRAMS SBBR (variants A, C, and D) broadband radiometer with hemispherical FOV; measures downwelling flux from 0.3 to 4 μm

(IOP instrument data to be supplied)

Satellite GOES-8:

Instrument 1: imager multi-channel instrument designed to sense radiant and solar-reflected energy from sampled areas of the Earth; produces full-Earth disc images

Satellite NOAA-12:

Instrument 1: AVHRR cross-track scanning system with five spectral channels; the spectral band widths are 0.58-0.68, 0.725-1.10, 3.55-3.93, 10.3-11.3, and 11.5-12.5 μm; IFOV of each channel is approximately 1.4 mrad leading to a resolution at the satellite sub-point of 1.1 km for a nominal altitude of 833 km; IR channels are calibrated in-flight; no in-flight visible channel calibration is performed

Satellite NOAA-14:

Instrument 1: AVHRR cross-track scanning system with five spectral channels; the spectral band widths are 0.58-0.68, 0.725-1.10, 3.55-3.93, 10.3-11.3, and 11.5-12.5 μm; IFOV of each channel is approximately 1.4 mrad leading to a resolution at the satellite sub-point of 1.1 km for a nominal altitude of 833 km; IR channels are calibrated in-flight; no in-flight visible channel calibration is performed

Experiment Group 2 Surface Characterization

Part A Science Issues

Science Objective

The objective of this group of experiments is to measure the effects of surface properties on the solar and infrared radiation budgets in the atmospheric column. Specific objectives include building databases of spectrally resolved BDRF viewed from the tropopause and spectrally resolved and broadband directional albedo models (DAM) viewed from near surface, and to determine the response of surface skin temperature to cloud shading.

Surface properties play an important role (I) in the atmospheric radiation budget and (ii) in the retrieval of derived products, such as cloud optical depth and cloud amount, from a variety of satellite spectral observations. Clear-sky reflectance (CSR) plays an essential role in the retrieval of derived products, such as cloud optical depth and cloud amount, from a variety of satellite spectral observations. BDRFs are typically used to specify the CSR because they can account for various viewing, illumination, and surface anisotropy conditions and, potentially, a variety of atmospheric aerosol loadings. The BDRFs for different surface types and wavelengths have been approximated from theoretical calculations for some surface conditions and measured near the surface or at high altitudes for a limited number of surface types and solar zenith angles. The objective of this experiment is to dramatically enhance the number and type of the empirical observations.

Surface albedo varies with sun angle, surface type, and the atmospheric conditions. Variation of the clear-sky albedo at the top of the atmosphere depends on these same parameters but in a different manner. In general, models assume that the surface albedo is constant when the sky is cloudy. However, the validity of that assumption may not hold in a variety of cloud conditions, especially for thin or broken clouds. This experiment will provide the data necessary to test that assumption under a range of cloud conditions and surface types. Furthermore, when conducted in clear skies, this experiment will provide the data needed to specify the ADM at the surface and near the top of the atmosphere for different surface types. These data will then be used to determine how accurately current models can compute the solar zenith angle dependence of clear-sky albedo, both spectral and broadband, given the surface albedo over a range of solar elevations. Both the clear-sky solar zenith angle albedo dependence and under-cloud surface albedos are essential quantities for accurate computation of atmospheric absorption.

The surface skin temperature (TS) is a critical parameter in satellite cloud retrieval and in the partitioning of surface-absorbed solar energy in the surface as latent, sensible, or stored heat. In satellite retrievals of cloud amounts and cloud properties, a particular value of skin temperature is usually assumed for a particular surface and time of day and year. The assumption either relies on measurements taken in a clear portion of the scene or on similar measurement taken at a previous time. Cloudy pixels are generally determined to be those with temperatures less than TS minus some tolerance, usually a standard deviation. Because such temperatures and standard deviations are taken in cloud-free conditions, they do not account for any reductions in temperatures for areas shaded by the clouds, but observed by the satellite. Thus, some shaded areas may be misinterpreted as "dark" clouds. In addition, the cloud-free (shade-free) values of TS are usually assumed to be the same as the temperature of the areas shaded by the clouds in partly cloudy conditions. These satellite-derived values of TS are those used in model calculations of the surface energy budgets. Improvements in accurate assessment of TS by accounting for the cloud-shaded areas in both overcast and partly cloudy conditions will help produce more accurate cloud retrievals and surface energy budget calculations as well as improved estimates of longwave cloud forcing.

Advocate

The Satellite Analysis Group advocates these experiments. Individuals desiring to analyze the data include Pat Minnis, Weigang Gao, Tom Charlock, and Zhangqing Li.

Measurement Strategy

All measurements will be taken at an altitude above 13.7 km or as close to the surface as possible for segments that cover half of the diurnal cycle (sunrise to noon or noon to sunset) for several days that include a variety of cloud conditions. The desired surfaces should include (i) the area centered on the CART site central facility (CF), (ii) bare soil possibly west of the CF, (iii) grassland east of the CF, (iv) mixed woodland southeast of the CF, (v) the length of Kaw Lake, and the (vi) Great Salt Plains salt flat. Satellite imagery will be used to characterize the spectral uniformity of a particular site. The most critical areas are those that are large enough to essentially fill both the hemispherical instruments fields of view for several measurements.

Variant A BDRF vs Time of Day

The BDRF of a cloud field or clear sky would ideally be obtained by averaging the spectrally and angularly resolved radiation emanating upward from many points on its or the surface. Of course, such a measurement is impractical. The reverse measurement is more tractable, that is, measuring the spectrally and angularly resolved radiation converging upward to a point well above the cloud field or earth s surface. Since for clouds this measurement involves radiation from many different elements on the its surface, it only makes sense for fields that meet some uniformity criteria. Such criteria can be expressed in terms of how smoothly the derived BDRF varies and the equality of equivalent angles on either side of the solar vector.

The MPIR will be used to gather raw data for 4 spectral bands resolved into approximately 256 polar angle bins between 0° and 66° from nadir and 200 azimuth angle bins from 0° to 360°. This will be accomplished by turning a 360° clockwise turn with a radius of 2.5 km at 15° bank with the MPIR canted 11° to the port. The measurement will take a little over 180 seconds. Aircraft motion plus wind differential between the cloud tops or surface and the aircraft s altitude cause the measurement to be made over an area of a few kilometers rather than the desired point.

All measurements will be taken in clear skies at an altitude of 13.7 km or greater for half of the diurnal cycle (sunrise to noon or noon to sunset) for several days. Flights should be made over surface types i, ii, iii, and iv. Additionally measurements will be made at 2 km over the CF near the beginning or end of a flight. The highest priority is for the high-altitude measurements. Aircraft antenna limitations may preclude flights in certain directions from the base airport.

Variant B Albedo vs Cloudiness and Sun Angle

This variant employs only the DHC-6 aircraft flying straight-line patterns over each of the surface types mentioned above. The aircraft altitude will be as low as conveniently possible. Desired meteorological conditions include clear, broken, and thin cloud conditions.

Variant C Skin Temperature

As in the above variant, only the DHC-6 aircraft is required, and it will fly straight-line patterns over all the mentioned surface types at as low an altitude as convenient. The necessary cloud field for this variant will produce large areas of shadow and sunlight on the surface such that the aircraft can fly between them having the hemispherical instruments field of view filled by the shaded or sunlit areas.

Required and Supporting Measurements

UAV

The critical instrument on this platform for variant A is the MPIR to make spectral radiance measurements. If simultaneous mounting with the MPIR is possible, the CDL will be used for detecting any thin clouds above or below the UAV. Variants B and C do not employ this platform.

Instrumented Chase

The primary instrument on this platform for variants B and C is the RAMS to make broadband irradiance and spectral flux measurements; the IR instrument heads will be needed for variant C. The SSP will be used for acquiring spectral flux data for variant B and as a rapid response instrument for detecting variations in shading conditions for variant C. A IRT (10 μm wavelength radiometer) in the nadir viewing configuration is highly desirable but unavailable for rapid measurement of the changing skin temperature, which must thus be deduced from IR broadband measurements.

Ground

MSRFR data is needed for estimating the aerosol optical depth of the atmospheric column for variants A and B. Balloon borne soundings will be used to characterize the atmospheric profile and surface level winds for the various surface sites for variants B and C. Several additional data sets are needed for variant C. These are the longwave radiometers and a down looking IRT on the radiometer tower (10 m) for evaluation of the atmospheric corrections of the aircraft measurements, the SW radiometers on the central facility tower for characterizing the shading conditions, and surface air temperatures at each target site.

Satellite

The supporting instruments are the infrared and visual imagery form GOES-8 imager or GOES-9 imager and the high-resolution AVHRR (NOAA-12 or NOAA-14) visible and near-infrared imagery and normalized vegetation indices to characterize surface type and spectral uniformity.

Data Analysis Strategy

Variant A BDRF vs Time of Day

Data from the MPIR will be averaged into a reduced set of 36 azimuthal bins and 7° zenith angle bins for each trial after normalization to the mean solar zenith angle for the trial. High-altitude measurements will corrected to the top of the atmosphere using radiative transfer modeling and appropriate gaseous loading in the stratosphere. Radiative transfer modeling will be used to correct the near-surface BDRFs to the top of the atmosphere using surface-derived aerosol loadings.

Variant B Albedo vs Cloudiness and Sun Angle

Upwelling and downwelling spectral and broadband fluxes from all of the flux radiometers will be averaged over a single trial. Spectral and broadband albedos will be computed for each trial and assigned the mean solar zenith angle (SZA) for the trial. Similar quantities will be computed for the SSP radiances using a Lambertian assumption. Radiative transfer modeling will be used to correct the near surface albedos to the surface using both gas and surface derived aerosol loadings. Similar measurements at the CF will be used to verify the DHC-6 to surface corrections for the CF over flights to estimate surface spectral albedos. Results from trials conducted over the same sites at different solar zenith angles will be used to construct a DAM for each surface type for both the surface and TOA. Measurements taken in clear conditions at the surface will be used as the lower boundary in a radiative model to compute the TOA albedo. The results at each SZA will be used to determine how well the model performs as a function of SZA. The measurements taken by the DHC-6 in cloudy conditions will be averaged in the same manner and compared to the diffuse assumptions currently used in model calculations. The SZA dependence of surface albedo will then be characterized in terms of cloud conditions and surface type. Cloud conditions will be quantified in terms of brokeness, optical depth, and phase using measurements from GOES satellites. Radiative transfer modeling will be used to estimate the errors in absorption due to current assumptions compared to actual SZA dependence of surface albedo.

Variant C Skin Temperature

Upwelling broadband LW fluxes from the DHC-6 RAMS will be averaged for each clear and shaded portion of a single trial. DHC-6 SSP data will be used to determine shading and clear conditions for each LW measurement. The data will be characterized in terms of the SZA, surface type, wind, and length of time of shading to estimate effect of each parameter on T_s. T_s will be estimated from the LW fluxes using radiative transfer modeling from the surface to flight level. The impact of the atmospheric radiation on the surface heating will also be estimated using the up looking RAMS LW radiometer on the top of the DHC-6. Similar quantities will be computed using the radiometry on the CF tower using time instead of length as an estimate of shadow size. Cloud optical depth and cloud cell size will be estimated from satellite data. Cloud height will be determined from the satellite and central facility data.

Relation to Other Experiments

Variant A is closely associated with experiment 10 of the ARM UAV Science and Experiment Plan, 1996 Flight Series, Revision 4, March 2, 1996.

Part B Experiment Details

Flight Strategy

Variant A BDRF vs Time of Day

The Altus will be flown to a point upwind of that indicated in Table 2 and then will accumulate data while turning three successive 360° clockwise turns at 15° bank angle. Since this maneuver will take approximately 10 minutes, wind drift is a consideration. Best judgement will be used to initially position the aircraft so that the aircraft s turning center is near the indicated point in the middle of the second turn.

All measurements will be taken in clear skies at an altitude of 13.7 km for half of the diurnal cycle (sunrise to noon or noon to sunset) over several days in conjunction with flights for other experiments. Flights should be made over surface types i, ii, iii, and iv. Additionally measurements will be made at 2 km over the CF near the beginning or end of a flight.

Variant B   Albedo vs Cloudiness and Sun Angle

This variant employs only the DHC-6 aircraft flying straight-line patterns over each of the six surface types between the end coordinates in Table 2. The aircraft altitude will be as low as conveniently possible. Desired meteorological conditions include clear, broken, and thin cloud conditions. Flights will be made at various times during the day to capture data for as wide a variety of solar zenith angles as possible.

Variant C   Skin Temperature

As in the above variant, the DHC-6 aircraft will fly straight-line patterns over each of the six surface types between the end coordinates in Table 2. The aircraft altitude will be as low as conveniently possible. Flights will be made at various times during the day to capture data for as wide a variety of solar zenith angles as possible. The necessary cloud field for this variant will produce large areas of shadow and sunlight on the surface such that the aircraft can fly between them having the hemispherical instruments field of view filled by the shaded or sunlit areas.

Constraints

The following table specifies the coordinates of the end points for each of the six terrain sets.

Table 2. Flight Path Definition for Surface Characterization

End Point	*UTM*	*Lat Long*

	I SGP CART Central Facility				
N	634810	4064248	14	36°42.9'N	97°29.4'W
BDRF	634999	4052249	14	36°36.3'N	97°29.4'W
S	635188	4040250	14	36°29.9'N	97°29.4'W
	II Bare Soil West of the Central Facility				
NE	634999	4052249	14	36°36.3'N	97°29.4'W
BDRF	624708	4043415	14	36°31.7'N	97°36.4'W
SW	614417	4034581	14	36°27.0'N	97°43.4'W
	III Grassland East of the Central Facility				
NW	698145	4090344	14	36°56.3'N	96°46.5'W
BDRF	708054	4083370	14	36°52.4'N	96°39.9'W
SE	717962	4076396	14	36°48.5'N	96°33.4'W
	IV Mixed Woodland Southeast of the Central Facility				
NE	752702	4002761	14	36°08.2'N	96°11.5'W
BDRF	743617	3994458	14	36°03.9'N	96°17.7'W
SW	734532	3986155	14	35°59.5'N	96°23.9'W
	V Kaw Lake				
WSW	685300	4066373	14	36°43.5'N	96°55.5'W
ENE	691175	4070018	14	36°45.4'N	96°51.5'W
	VI Great Salt Plains Salt Flat				
WSW	563980	4066640	14	36°44.6'N	98°17.0'W

ENE	571823	4071879	14	36°47.4'N	98°11.7'W

Special Needs

The MPIR will be canted 11° to the port side on the Altus.

Instrument and Data List

UAV

Instrument 1: MPIR (variant A) four channels (0.62-0.67 μm, 0.86-0.90 μm, 1.36-1.39 μm, and 1.58-1.64 μm) each yielding data from a 256 element linear array (512 element for band 1) that is oriented to provide a curved, across track radiometric line image; the line images are spatially co-registered and temporally sampled each 0.5 second (0.25 for band 1); the instantaneous FOV for each pixel is 6 mrad (3 mrad for band 1)

Instrument 2: CDL (variant A) 200 range bins with intensity of reflected laser light plus one background bin; range bins provide information on the location and density of aerosols and clouds; background bin for data correction

Instrumented Chase

Instrument 1: nadir SSP1 (variants B and C) reflected spectral radiance in $Wm^{-2}sr^{-1}nm^{-1}$, 0.4 to 4.0 μm; reflected spectral flux in $Wm^{-2}nm^{-1}$, 0.4 to 2.5 μm; 2 channels linearly polarized (||, ⊥) reflected spectral radiance in $Wm^{-2}sr^{-1}nm^{-1}$, 0.4 to 2.5 μm

Instrument 2: zenith TDDR (variants B and C) downwelling hemispherical flux data; seven channels each 10 nm wide; channel center wavelengths are 0.5, 0.86, 1.0, 1.25, 1.5, 1.65, and 1.75 μm; shadow rings move across the FOV periodically blocking direct solar radiation thus enabling determination of the diffuse : direct ratio

Instrument 3: nadir TDDR (variants B and C) upwelling hemispherical flux data; seven channels each 10 nm wide; channel center wavelengths are 0.5, 0.86, 1.0, 1.25, 1.5, 1.65, and 1.75 μm

Instrument 4: zenith FSBBR (variants B) broadband radiometer with hemispherical FOV; measures downwelling flux from 0.7 to 3 μm

Instrument 5: nadir FSBBR (variants B) broadband radiometer with hemispherical FOV; measures upwelling flux from 0.7 to 3 μm

Instrument 6: zenith IRBBR (variant C) broadband radiometer with hemispherical FOV; measures downwelling flux from 0.7 to 3 μm

Instrument 7: nadir IRBBR (variant C) broadband radiometer with hemispherical FOV; measures upwelling flux from 0.7 to 3 μm

Instrument 8: zenith SBBR (variants B and C) broadband radiometer with hemispherical FOV; measures downwelling flux from 0.3 to 4 μm

Instrument 9: nadir SBBR (variants B and C) broadband radiometer with hemispherical FOV; measures upwelling flux from 0.3 to 4 μm

Ground

Instrument 1: Lamont MFRSR (variants A and B) hemispheric downward solar irradiance (415, 500, 610, 665, 862, and 940 nm); hemispherical downward total solar irradiance; diffuse hemispherical downward solar irradiance (415, 500, 610, 665, 862, and 940 nm) diffuse hemispherical downward total solar irradiance; direct beam normal solar irradiance (415, 500, 610, 665, 862, and 940 nm); and direct beam normal total solar irradiance

Instrument 2: radiosonde (variants B and C) balloon borne instrument measuring temperature, pressure, water vapor, and winds from its surface launch point upwards to a 35 km altitude during a 2 hour period

Instrument 3: nadir IRT (variant C) ground-based radiation pyrometer that provides measurements of the equivalent black body brightness temperature of the scene in its field of view; has a wide field of view for measuring the narrowband rotating temperature of the ground surface

Instrument 4: Lamont SMOS (variant C) *in situ* sensors to obtain one-minute and thirty-minute averages of surface wind speed, wind direction, air temperature, relative humidity, barometric pressure, and precipitation at the central facility; snow depth is also measured with an ultrasonic device

Instrument 5: Lamont SIRS (variant C) direct beam normal solar irradiance; downwelling diffuse solar irradiance; downwelling hemispherical solar irradiance; upwelling hemispherical solar irradiance; downwelling hemispherical infrared radiance

Satellite GOES-8:

Instrument 1: imager (visible) (all variants) multi-channel instrument designed to sense radiant and solar-reflected energy from sampled areas of the Earth; produces full-Earth disc images with 1 km resolution

Instrument 2: imager (infrared) (all variants) multi-channel instrument designed to sense radiant and solar-reflected energy from sampled areas of the Earth; produces full-Earth disc images with 4 km resolution

Satellite GOES-9:

Instrument 1: imager (visible) (all variants) multi-channel instrument designed to sense radiant and solar-reflected energy from sampled areas of the Earth; produces full-Earth disc images with 1 km resolution

Instrument 2: imager (infrared) (all variants) multi-channel instrument designed to sense radiant and solar-reflected energy from sampled areas of the Earth; produces full-Earth disc images with 4 km resolution

Satellite NOAA-12:

Instrument 1: AVHRR (all variants) cross-track scanning system with five spectral channels; the spectral band widths are 0.58-0.68, 0.725-1.10, 3.55-3.93, 10.3-11.3, and 11.5-12.5 μm; IFOV of each channel is approximately 1.4 mrad leading to a resolution at the satellite sub-point of 1.1 km for a nominal altitude of 833 km; IR channels are calibrated in-flight; no in-flight visible channel calibration is performed

Satellite NOAA-14:

Instrument 1: AVHRR (all variants) cross-track scanning system with five spectral channels; the spectral band widths are 0.58-0.68, 0.725-1.10, 3.55-3.93, 10.3-11.3, and 11.5-12.5 μm; IFOV of each channel is approximately 1.4 mrad leading to a resolution at the satellite sub-point of 1.1 km for a nominal altitude of 833 km; IR channels are calibrated in-flight; no in-flight visible channel calibration is performed

Experiment 3 ARESE Re-reprise

Part A Science Issues

Science Objective

The objective is to determine if cloudy atmospheres absorb more shortwave radiation than predicted by state-of-the-art climate models.

The ARESE experiment was conducted in the fall 1995 ARM-UAV campaign, and a reprise of that experiment was proposed in the 1996 science plan[1]. This experiment is a follow-on to that campaign and reprise experiments. The original experiment was developed fully in a separate report[2]. This document contains only a summary description from that science plan and is adapted to a follow-on effort.

Two objectives are imbedded in this hypothesis: (1) the direct measurement of the absorption of solar radiation by clear and cloudy atmospheres and the placement of bounds on these measurements and (2) the investigation of the possible causes of absorption in excess of model predictions.

Evidence from several experimental and theoretical investigations over the past four decades has shown that the magnitude of shortwave absorption by clouds is uncertain. There has been some evidence that absorption is more than that predicted by models. F. Valero and several other investigators have concluded that the absorption by the entire atmospheric column in the presence of clouds exceeds model predictions of absorption by perhaps 35 W/m^2 (day side average) over the Pacific warm pool. The relative error this presents in current theoretical estimates of solar absorption is large, considering that average clear-sky absorption in that region is about 100 W/m^2 (dayside average). The absolute error appears to be small when compared to other terms in the energy budget, but that is misleading. Most of the solar radiation absorbed in the tropics goes toward heating the surface, the remainder, about 20%, helps drive the atmospheric circulation. Thus, what appear to be small errors in absorption by the atmosphere might have huge consequences in tropical atmospheric dynamics. Another consequence of the inadequacy of our understanding of solar absorption by clouds is the misinterpretation of remote sensing data used to infer cloud microphysical properties.

The fall 1995-ARESE experiment produced data from 12 science flights, which have been analyzed and presented in various journal and meeting papers. The results appear to strongly support the hypothesis, but have been challenged in their details. The subject of this re-reprise experiment is the filling of any gaps in the earlier data, if such filling is essential to the understanding of the hypothesis as indicated by preliminary analyses. If either the differing UAV instrument suite or extant meteorological conditions will not produce significantly improved data from that already taken, then this experiment will not be undertaken.

Advocate

The original ARESE experiment had its own separate science team. The chair of this team and chief scientist was Francisco Valero from Scripps Oceanographic Institute. Stephen Schwartz from Brookhaven National Laboratory and later John Vitko, Jr. from Sandia National Laboratories were the project directors. The champion for this re-reprise experiment is Francisco Valero. The individuals involved in data analysis are Francisco Valero, Robert Cahalan, Catherine Gautier, Kuo-Nan Liou, Patrick Minnis, Shelly Pope, Stephen Schwartz, Graeme Stephens, Warren Wiscombe, Robert Cess, Jeff Kiehl, and Ram Ramanathan.

Measurement Strategy

The experimental emphasis of ARESE and this re-reprise focuses on the measurement of atmospheric column absorption through the acquisition of fluxes at different altitudes in the atmosphere and at the surface. This will be achieved by using satellite, aircraft, and ground observational platforms. The aircraft will cover the range from the tropopause to the low troposphere. Ground observations will be made from the ARM CART central and extended facilities, which are part of the ARM SGP site. Radiances measured by both GOES and NOAA series satellites will be compared to fluxes measured by aircraft at the tropopause, and then used to retrieve TOA fluxes.

The ARESE strategy involves the acquisition of radiometric data with multiple, coordinated aircraft and from the ground. The aircraft will fly tracks over the ground stations stacked at different altitudes. In this manner, it will be possible to obtain coeval measurements of radiative fluxes from which the absorption of radiation by the atmosphere can be estimated. Additionally, the aircraft sampling from the tropopause will be able to measure the reflectivity of the cloudy and clear atmospheres, and the surface observations will provide the radiative flux transmitted through the column. The top of the troposphere reflectivity and surface transmissivity values provide an additional indication of the magnitude of absorption by the atmospheric column.

Upper tropospheric measurements will be made from a UAV and lower tropospheric measurements from an ARM-UAV DHC-6 Twin Otter. Both aircraft will be equipped with identical Valero radiometers, as will be the SGP central facility. The original experiment had an additional aircraft at the tropopause, the NASA ER-2 similarly equipped with Valero radiometers.

Required and Supporting Measurements

The list of measurements to be made as part of this ARESE follow-on experiment are not as extensive as for the original experiment, which were fully covered in the ARESE science plan and is modified from that of the reprise experiment. Common to both aircraft is a RAMS for the characterization of shortwave and longwave upwelling and downwelling fluxes at their respective flight altitudes. The components of a RAMS are a) zenith SBBR, b) nadir SBBR, c) zenith FSBBR, d) nadir FSBBR, e) zenith TDDR (7 channels: 0.500, 0.865, 1.05, 1.25, 1.50, 1.65, and 1.75 μm), and f) nadir TDDR (7 channels: 0.500, 0.865, 1.05, 1.25, 1.50, 1.65, and 1.75 μm). For ground based measurements a zenith GRAMS system is used consisting of items a, c, and e.

UAV

The UAV will measure upwelling and downwelling solar fluxes in the upper troposphere with a RAMS. Additional supporting instrumentation a nadir SSP2 for collection of spectrally resolved 0.4 to 4.0 μm radiances from features directly below the aircraft and the MPIR for clouds image data in bands centered on 0.65, 0.88, 1.37, and 1.61 μm. The MPIR s cross track FOV will be ±40°.

Instrumented Chase

The DHC-6 will also measure upwelling and downwelling solar fluxes, but in the lower troposphere, with a RAMS. The additional on board supporting instrumentation is a zenith SSP1 for collection of spectrally resolved 0.4 to 1.0-μm radiances from features directly above the aircraft.

Ground

The Lamont GRAMS will measure downwelling solar fluxes at the SGP CART central facility. The Lamont SIRS, Lamont MFRSR, Byron SIRS, Byron MFRSR, Ringwood SIRS, Ringwood MFRSR, Coldwater SIRS, Coldwater MFRSR, Vici SIRS, and Vici MFRSR will augment these flux measurements; these radiation measurements will be primary at the four extended facilities over which flights will be made. Radiosondes launched from the central facility will characterize atmospheric water vapor and temperature. Several additional measurements will be made near the central facility, including (1) an augmentation of the sonde's water vapor by a Raman LIDAR system, (2) cloud extents and DD or ID with a millimeter wave cloud Doppler radar, (3) lower troposphere wind, temperature, and humidity conditions with both a 915 MHz profiler with RASS and 50 MHz profiler with RASS and (4) LW path with a MWR.

Satellite

The primary instrument is the imager on GOES-8 for measurement of narrowband radiances in the visible and infrared bands. Secondarily, narrowband data will be used from the imager (GOES-9) and AVHRR

(NOAA-12, and NOAA-14), whenever satellite views match the area of operations.

Data Analysis Strategy

The data taken in any re-reprise experiment will be used to supplement data already acquired in the Fall 1995 campaign and in the reprise experiments during 1996 campaigns. The data analysis strategy associated with the ARESE campaign will be used also for the additional data and is reviewed herein, with appropriate modifications for the reduced aircraft suite and changed instrument suites.

Three strategies will be used for evaluating cloudy sky atmospheric absorption relative to models. These can be variously adapted to use data from the four levels of ARESE reprise measurements: (1) surface, (2) 0.5 km DHC-6, (3) 12 km UAV, and (4) TOA (satellite).

A direct way of evaluating cloudy sky shortwave absorption, relative to that for clear skies, is to compare cloud radiative forcing at the surface to that at the TOA. Cloud radiative forcing is the difference between all-sky and clear sky net downward shortwave radiation. Models typically give a value near one for the ratio of cloud radiative forcing at the surface to cloud radiative forcing at the TOA although some recent measurements indicate a value near 1.5 might be more appropriate. Since model simulations of cloud radiative forcing are easily performed for the DHC-6 and Altus UAV altitudes, this approach can be used to compare measurements taken on board those platforms with model results.

During this ARESE re-reprise upwelling surface shortwave flux will not be measured with the same instruments used on board the aircraft since the zenith GRAMS used on the surface (and only at the central facility) has no nadir viewing components. A second analysis strategy overcomes this deficiency by substituting surface insolation for the surface net flux used in the above strategy. Models typically give a value near 1.25 for the ratio of surface cloud insolation forcing to TOA cloud radiative forcing, compared to some recent measurements indicating a value nearer 1.75 for this same ratio.

The ratio of cloud radiative forcing at the surface to that at the TOA can be shown to be mathematically equal to $-(\Delta\alpha/\Delta T)^{-1}$ where α is the

TOA albedo and T is the atmospheric transmittance. This leads to a third approach that evaluates $\Delta\alpha/\Delta T$ from a linear regression of the measured quantities of albedo and transmittance. Since this approach does not require clear sky identification, it serves to remove cloud shortwave absorption from broken cloud effects.

Relation to Other Experiments

As mentioned above, this experiment is a re-reprise of the ARESE experiment and its reprises which were fully developed in the separate documents.

Part B Experiment Details

Flight Strategy

The upper troposphere UAV will be used as an above cloud platform and the DHC-6 as a lower troposphere, below cloud platform. The mission of these aircraft is to provide measurements of net fluxes at 12 km and 0.8-km MSL, respectively, in both cloudy and clear sky conditions. These two aircraft will fly in coordination with their horizontal distance ideally not exceeding 4 km.

The original ARESE flight plan involved two long paths and a shorter triangular one, as shown in Figure 2. These same paths will be available for this re-reprise experiment. On any given flight day both aircraft will fly one of three standard tracks, with the particular one selected the previous evening based on forecast cloud and upper tropopause wind conditions as well as on instrument readiness and satellite calibration opportunities. The wind conditions affect the ability of the Altus UAV and DHC-6 to maintain coordinated flight. All three tracks over fly the CART central facility and selected extended facilities to insure periodic stacking of measurement assets in a column.

The 10-km full width flight corridors associated with all three of these tracks as well as 20 km diameter turning circles are shown in the figure. These corridors provide safe operating margins and represent regions for which flight approval will be sought. They have been chosen to avoid as much as possible over flight of small cities and towns in the area.

The first flight track is a triangle with vertices at the CART central facility (Lamont SIRS), and at the Ringwood and Byron extended facilities. The flight path lengths are (beginning with the central facility and heading toward Ringwood, including the dogleg) 75 km, 50 km, and 78 km.

The second flight track is near linear between the central facility and the Coldwater extended facility, flying over the Byron site along the way. The flight path including a slight bend is 182 km long in the WNW   ESE direction.

The third flight track is also near linear between the central facility and the Vici extended facility, flying over the Ringwood site along the way. The flight path including two slight bends is 163 km long in the WSW   ENE direction.

Constraints

No special conditions are defined for this reprise experiment.

Special Needs

There are no special needs for this experiment.

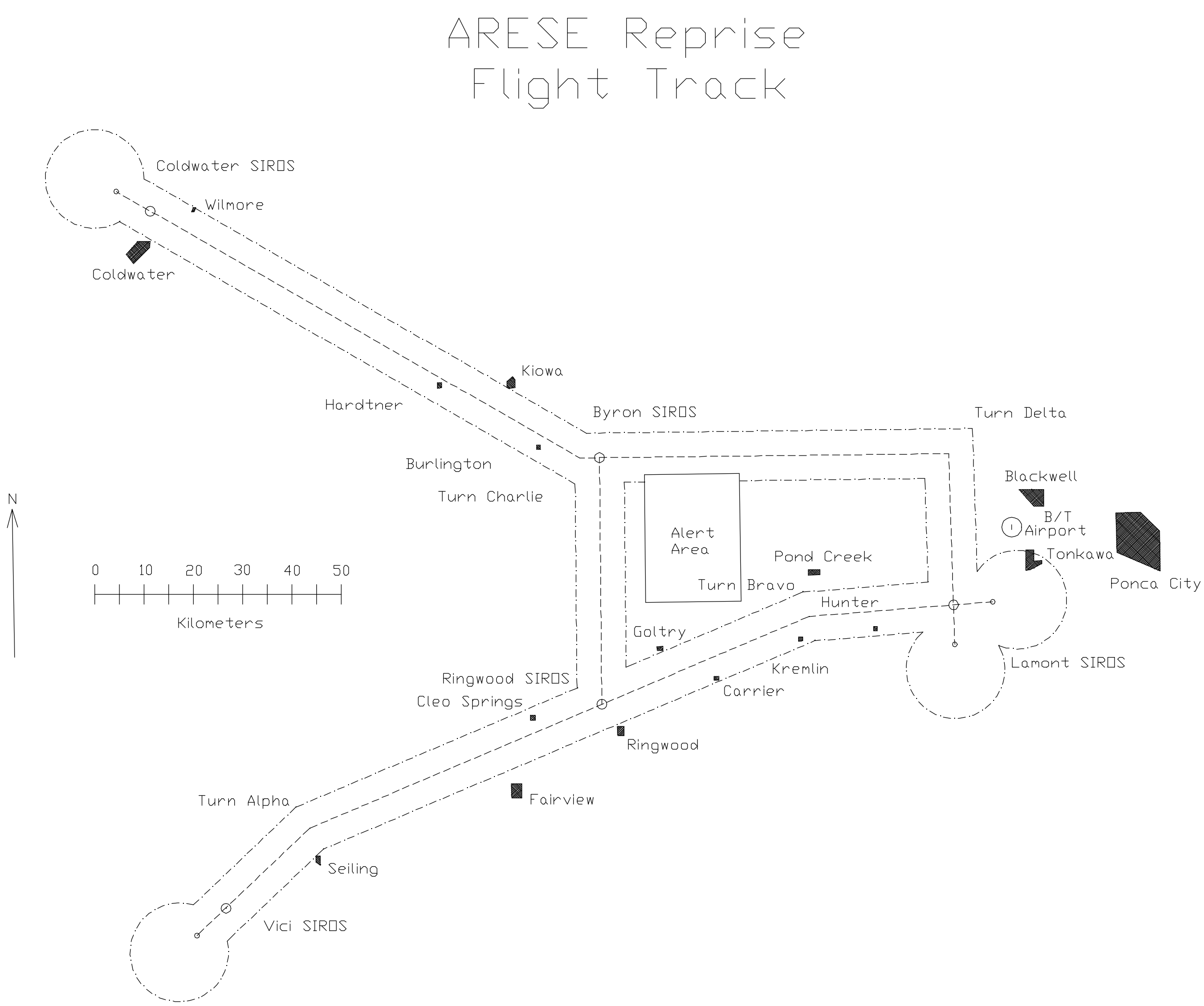

Figure 2. ARESE Re-reprise Flight Tracks.

Instrument and Data List

UAV

Instrument 1: MPIR four channels (0.62-0.67 μm, 0.86-0.90 μm, 1.36-1.39 μm, and 1.58-1.64 μm) each yielding data from a 256 element linear array (512 element for band 1) that is oriented to provide a curved, across track radiometric line image; the line images are spatially co-registered and temporally sampled each 0.5 second (0.25 for band 1); the instantaneous FOV for each pixel is 6 mrad (3 mrad for band 1)

Instrument 2: zenith TDDR downwelling hemispherical flux data; seven channels each 10 nm wide; channel center wavelengths are 0.5, 0.86, 1.0, 1.25, 1.5, 1.65, and 1.75 μm; shadow rings move across the FOV periodically blocking direct solar radiation thus enabling determination of the diffuse : direct ratio

Instrument 3: nadir TDDR upwelling hemispherical flux data; seven channels each 10 nm wide; channel center wavelengths are 0.5, 0.86, 1.0, 1.25, 1.5, 1.65, and 1.75 μm

Instrument 4: zenith FSBBR broadband radiometer with hemispherical FOV; measures downwelling flux from 0.7 to 3 μm

Instrument 5: nadir FSBBR broadband radiometer with hemispherical FOV; measures upwelling flux from 0.7 to 3 μm

Instrument 6: zenith SBBR broadband radiometer with hemispherical FOV; measures downwelling flux from 0.3 to 4 μm

Instrument 7: nadir SBBR broadband radiometer with hemispherical FOV; measures upwelling flux from 0.3 to 4 μm

Instrument 8: nadir SSP2 reflected spectral radiance in $Wm^{-2}sr^{-1}nm^{-1}$, 0.4 to 4.0 μm; reflected spectral flux in $Wm^{-2}nm^{-1}$, 0.4 to 2.5 μm; 2 channels linearly polarized (||, ⊥) reflected spectral radiance in $Wm^{-2}sr^{-1}nm^{-1}$, 0.4 to 2.5 μm; reflected broadband radiance in $Wm^{-2}sr^{-1}$, 0.4 to 4.0 μm; reflected broadband flux in Wm^{-2}, 0.4 to 2.5 μm

Instrumented Chase

Instrument 1: zenith TDDR downwelling hemispherical flux data; seven channels each 10 nm wide; channel center wavelengths are 0.5, 0.86, 1.0, 1.25, 1.5, 1.65, and 1.75 μm; shadow rings move across the FOV periodically blocking direct solar radiation thus enabling determination of the diffuse : direct ratio

Instrument 2: nadir TDDR upwelling hemispherical flux data; seven channels each 10 nm wide; channel center wavelengths are 0.5, 0.86, 1.0, 1.25, 1.5, 1.65, and 1.75 μm

Instrument 3: zenith FSBBR broadband radiometer with hemispherical FOV; measures downwelling flux from 0.7 to 3 μm

Instrument 4: nadir FSBBR broadband radiometer with hemispherical FOV; measures upwelling flux from 0.7 to 3 μm

Instrument 5: zenith SBBR broadband radiometer with hemispherical FOV; measures downwelling flux from 0.3 to 4 μm

Instrument 6: nadir SBBR broadband radiometer with hemispherical FOV; measures upwelling flux from 0.3 to 4 μm

Instrument 7: zenith SSP1 reflected spectral radiance in $Wm^{-2}sr^{-1}nm^{-1}$, 0.4 to 4.0 μm; reflected spectral flux in $Wm^{-2}nm^{-1}$, 0.4 to 2.5 μm; 2 channels linearly polarized (||, ⊥) reflected spectral radiance in $Wm^{-2}sr^{-1}nm^{-1}$, 0.4 to 2.5 μm

Ground

Instrument 1: Raman LIDAR 355 nm laser system providing profiles of water vapor, aerosols, and optically thin clouds with 40 meter resolution; maximum altitude for water vapor is 4 km daytime and 10 km night time; maximum altitude for aerosols and clouds is 15 km

Instrument 2: radiosonde balloon borne instrument measuring temperature, pressure, water vapor, and winds from its surface launch point upwards to a 35 km altitude during a 2 hour period

Instrument 3: MMCR (all variants) zenith-pointing radar that operates at a frequency of 35 GHz to determine cloud boundaries (e.g., cloud bottoms and tops) and radar reflectivity (dBZ) of the atmosphere up to 20 km; has a Doppler capability that will allow the measurement of cloud constituent vertical velocities

Instrument 4: 915 MHz profiler with RASS profiles of virtual temperature, wind speed, and wind direction

Instrument 5: 50 MHz profiler with RASS profiles of virtual temperature, wind speed, and wind direction

Instrument 6: MWR water vapor density profile and five-minute averages of column integrated water vapor, column integrated liquid water, and blackbody equivalent brightness temperature

Instrument 7: Lamont GRAMS TDDR downwelling hemispherical flux data; seven channels each 10 nm wide; channel center wavelengths are 0.5, 0.86, 1.0, 1.25, 1.5, 1.65, and 1.75 μm; shadow rings move across the FOV periodically blocking direct solar radiation thus enabling determination of the diffuse: direct ratio

Instrument 8: Lamont GRAMS FSBBR broadband radiometer with hemispherical FOV; measures downwelling flux from 0.7 to 3 μm

Instrument 9: Lamont GRAMS SBBR broadband radiometer with hemispherical FOV; measures downwelling flux from 0.3 to 4 μm

Instrument 10: Lamont SIRS direct beam normal solar irradiance; downwelling diffuse solar irradiance; downwelling hemispherical solar irradiance; upwelling hemispherical solar irradiance; downwelling hemispherical infrared radiance

Instrument 11: Lamont MFRSR hemispheric downward solar irradiance (415, 500, 610, 665, 862, and 940 nm); hemispherical downward total solar irradiance; diffuse hemispherical downward solar irradiance (415, 500, 610, 665, 862, and 940 nm) diffuse hemispherical downward total solar irradiance; direct beam normal solar irradiance (415, 500, 610, 665, 862, and 940 nm); and direct beam normal total solar irradiance

Instrument 12: Byron SIRS direct beam normal solar irradiance; downwelling diffuse solar irradiance; downwelling hemispherical solar irradiance; upwelling hemispherical solar irradiance; downwelling hemispherical infrared radiance

Instrument 13: Byron MFRSR hemispheric downward solar irradiance (415, 500, 610, 665, 862, and 940 nm); hemispherical downward total solar irradiance; diffuse hemispherical downward solar irradiance (415, 500, 610, 665, 862, and 940 nm) diffuse hemispherical downward total solar irradiance; direct beam normal solar irradiance (415, 500, 610, 665, 862, and 940 nm); and direct beam normal total solar irradiance

Instrument 15: Ringwood SIRS direct beam normal solar irradiance; downwelling diffuse solar irradiance; downwelling hemispherical solar irradiance; upwelling hemispherical solar irradiance; downwelling hemispherical infrared radiance

Instrument 16: Ringwood MFRSR hemispheric downward solar irradiance (415, 500, 610, 665, 862, and 940 nm); hemispherical downward total solar irradiance; diffuse hemispherical downward solar irradiance (415, 500, 610, 665, 862, and 940 nm) diffuse hemispherical downward total solar irradiance; direct beam normal solar irradiance (415, 500, 610, 665, 862, and 940 nm); and direct beam normal total solar irradiance

Instrument 17: Vici SIRS direct beam normal solar irradiance; downwelling diffuse solar irradiance; downwelling hemispherical solar irradiance; upwelling hemispherical solar irradiance; downwelling hemispherical infrared radiance

Instrument 18: Vici MFRSR hemispheric downward solar irradiance (415, 500, 610, 665, 862, and 940 nm); hemispherical downward total solar irradiance; diffuse hemispherical downward solar irradiance (415, 500, 610, 665, 862, and 940 nm) diffuse hemispherical downward total solar irradiance; direct beam normal solar irradiance (415, 500, 610, 665, 862, and 940 nm); and direct beam normal total solar irradiance

Instrument 19: Coldwater SIRS direct beam normal solar irradiance; downwelling diffuse solar irradiance; downwelling hemispherical solar irradiance; upwelling hemispherical solar irradiance; downwelling hemispherical infrared radiance

Instrument 20: Coldwater MFRSR hemispheric downward solar irradiance (415, 500, 610, 665, 862, and 940 nm); hemispherical downward total solar irradiance; diffuse hemispherical downward solar irradiance (415, 500, 610, 665, 862, and 940 nm) diffuse hemispherical downward total solar irradiance; direct beam normal solar irradiance (415, 500, 610, 665, 862, and 940 nm); and direct beam normal total solar irradiance

Satellite GOES-8:

Instrument 1: imager multi-channel instrument designed to sense radiant and solar-reflected energy from sampled areas of the Earth; produces full-Earth disc images

Satellite GOES-9:

Instrument 1: imager multi-channel instrument designed to sense radiant and solar-reflected energy from sampled areas of the Earth; produces full-Earth disc images

Satellite NOAA-12:

Instrument 1: AVHRR cross-track scanning system with five spectral channels; the spectral band widths are 0.58-0.68, 0.725-1.10, 3.55-3.93, 10.3-11.3, and 11.5-12.5 μm; IFOV of each channel is approximately 1.4 mrad leading to a resolution at the satellite sub-point of 1.1 km for a nominal altitude of 833 km; IR channels are calibrated in-flight; no in-flight visible channel calibration is performed

Satellite NOAA-14:

Instrument 1: AVHRR cross-track scanning system with five spectral channels; the spectral band widths are 0.58-0.68, 0.725-1.10, 3.55-3.93, 10.3-11.3, and 11.5-12.5 μm; IFOV of each channel is approximately 1.4 mrad leading to a resolution at the satellite sub-point of 1.1 km for a nominal altitude of 833 km; IR channels are calibrated in-flight; no in-flight visible channel calibration is performed

Experiment 4 Diurnal Radiation Budget Quantities

Part A Science Issues

Science Objective

Study the effect of diurnal cycles on the radiation budget.

In the absence of large synoptic changes, e.g. frontal passages, the radiation and cloud fields can be dominated by the diurnal cycle. These changes occur on many scales. Previous measurements of the outgoing radiation budget at the top or near the top of the atmosphere have been limited to only a few times of day at large scales. Complete diurnal cycles of the radiation field have only been estimated from narrowband radiance data taken by geostationary satellites. Current plans for the CERES experiment involve the use of geostationary data normalized to the twice per day CERES broadband data to cover the entire diurnal cycle. This approach needs to be verified. The geostationary data are limited to only one viewing zenith angle and rarely view at relative azimuth angles less that 70°. It is important to know not only how the radiation field varies as a whole over the day, but also how it varies with viewing angles on a diurnal basis. Furthermore, the variations in atmospheric constituents affecting the radiation field need to be measured to understand why the radiation field changes as it does and how the water is distributed both vertically and horizontally as the day progresses. Understanding the diurnal cycle of clouds and radiation at various scales will be very useful for improved monitoring and modeling of clouds and the radiation budget.

Advocate

Pat Crowley and Bob Ellingson support this experiment.

Measurement Strategy

Addressing this issue requires the near full time monitoring for two full diurnal cycles of the cloud fields within a test cell and radiation fields at the top of that cell, i.e., the tropopause. The monitoring period should not include any large-scale synoptic changes. The cell size should be at least 20 × 20 km and should be centered over the SGP CART central facility to take advantage of data provided by the extensive ground instrumentation there. Narrowband radiance data from both GOES and NOAA series satellites in the visible (0.55 to 0.75 μm), mid-near-infrared (0.85 to 1.6 μm), near-infrared (3.6 to 4.0 μm), and infrared (10.0 to 12.8 μm) bands will be used for testing the hypothesis.

Long duration UAV flights will be used to map the diurnal variations in the radiation field at the top of the cell. Broadband hemispherical fluxes may be obtained from a combination of Valero radiometers. Radiance measurements in nine narrow bands from the visible to infrared will be made with the MPIR. This instrument will be mounted so that the center of its FOV is 11° to the port side of the UAV, insuring that some of its pixels can match the VZA of the GOES-8 geostationary satellite when the UAV is flying in the proper direction. It is not possible to match the GOES-9 VZA at the SGP CART site with this instrument. The SSP mounted in nadir mode will provide spectrally resolved radiance measurements between 0.4 and 4.0 μm but only for a VZA near 0°.

Time varying cloud field morphological and microphysical data are needed to support subsequent data analysis. The former data set includes cloud three-dimensional structure for features larger than a few hundred meters and the latter set includes d, w, and phase for the same size features. This time dependent characterization will be obtained from a combination of ground, air, and space instrumentation, each of which provides only a portion of the overall representation. Retrieving the desired quantities will be a challenging task.

Knowing the atmospheric conditions in the cell is important for modeling the radiation fluxes observed. The most important datum in this regard is the time dependent water vapor profile; periodic radiosonde launches will be the basis for obtaining this, and they will be supplemented by a RASS system and a Raman LIDAR. In addition, the aerosol loading within and above the cell must be ascertained.

Required and Supporting Measurements

UAV

The primary instrument for measuring radiative fluxes at the tropopause will be the following combination of Valero radiometers: zenith SBBR, nadir SBBR, zenith IRBBR, nadir IRBBR, and zenith TDDR. The other primary instruments on this platform are (1) the MPIR, to be used to measure radiances in bands centered on 0.65, 0.88, 1.37, and 1.61 μm for retrieval of W, D, and phase as well as to assess the morphological variability of the cloud field through the variability of the radiance field, (2) the CDL for measurement of aerosol profiles above and below the UAV and mapping the cloud top height below, and (3) the SSP2 for spectrally resolved radiances at 0° VZA in the band 0.4 to 4.0 μm and polarization data for the retrieval of cloud phase.

Ground

Ground instrumentation will be located in the SGP central facility. The two primary instruments supporting the retrieval of cloud microphysical data are a 35 GHz cloud radar and MWR for measurement of D and W, respectively. An uplooking IRT aids in the extraction of IW and ID from radar data. Time dependent cloud morphological data at the few hundred meter resolution will be acquired from the radar just mentioned and a whole sky imager. A Raman LIDAR will be used to profile aerosol loading as well as to support radiosondes in profiling water vapor and temperature. In addition, for the lower troposphere, a 915 MHz profiler with RASS and 50 MHz profiler with RASS will aid in profiling temperature and humidity. The aerosol loading in the atmospheric column will be obtained from MFRSR readings. Finally, the Lamont SIROS will provide broadband flux data at the surface and the AERI narrowband infrared radiance. Surface temperature and emissivity is needed over the cell, however, no currently deployed instrument measures these quantities well.

Satellite

The primary instrument is the imager on either GOES-8 or GOES-9 for measurement of radiances in the visible, mid-near-infrared, near-infrared, and infrared bands. Supporting measurements from the AVHRR on NOAA-12 and NOAA-14 during over flights will provide the data in the same bands. Visual imagery from either the GOES-8 or GOES-9 will aid in the retrieval of large-scale cloud morphology.

Data Analysis Strategy

Two distinct data analyses will be undertaken. First, the various cloud morphological and microphysical data will be assembled together with atmospheric state parameters to predictively model the time varying radiative fluxes and radiances at the top of the cell. These will be compared to those measured by the UAV. Second, an interpolation of the measured satellite radiances will be used to generate a complete time history of radiances and fluxes at the tropopause. These will be compared to the measured values.

Relation to Other Experiments

This experiment is closely associated with experiment 11 of the ARM UAV Science and Experiment Plan, 1996 Flight Series, Revision 4, March 2, 1996.

Part B Experiment Details

Flight Strategy

This experiment will be flown once for two consecutive diurnal cycles that contain no large synoptic event. The flight may be interrupted briefly for UAV refueling and refurbishment. The flight level will be

14 km; this flight level determines the size of the experimental cell as explained below.

The center of the square experimental cell is coincident with the SGP CART central facility tower and its edges are either parallel or perpendicular to a locating line connecting the tower and the GOES-8 satellite nadir point. Any GOES-9, NOAA-12, or NOAA-14 data used will be navigated to this GOES-8 aligned square.

The flight path will be the edges of this square flown counterclockwise when viewed from the top so that the MPIR is always viewing into the cell. With the flight altitude of 14 km and with typical cloud tops in the cell at 4 km, the center of the MPIR FOV is offset 1.9 km from the flight track and the far edge is offset 12.3 km. Thus, the cell should be a 20-km square allowing for a 4.6-km square overlap region at the center. The accompanying figure shows the defined path.

Diurnal Radiation Budget
Flight Path

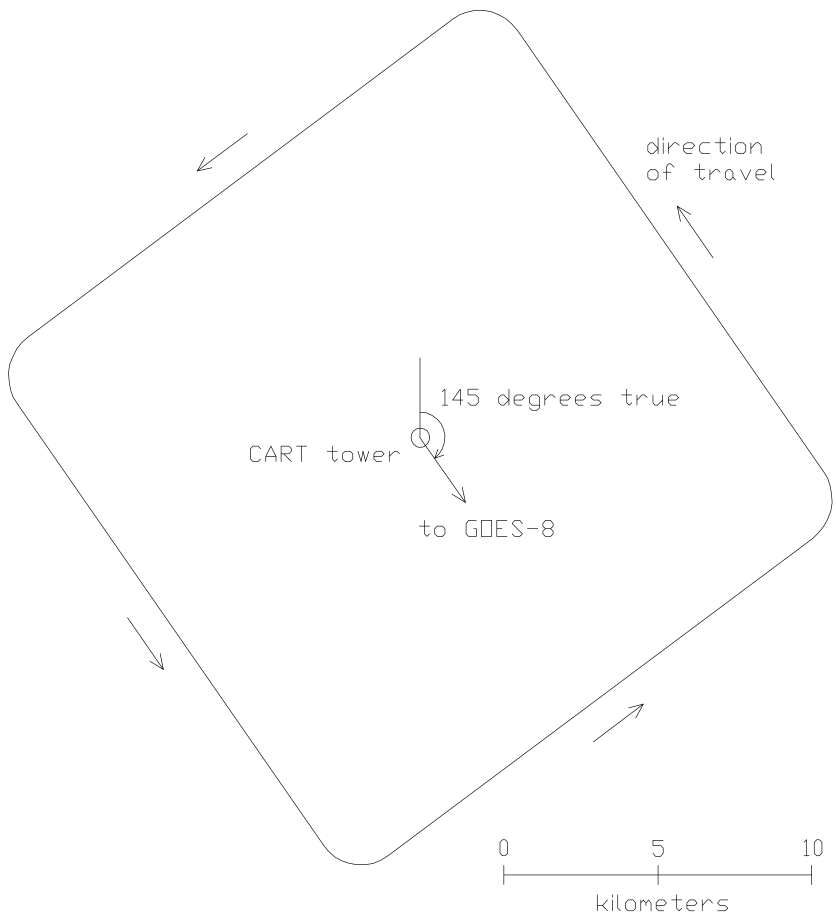

Constraints

The critical datum for the defining geostationary satellite is the azimuth angle (from north) of the line connecting the SGP CART central facility and the satellite nadir point.

General Geosynchronous Data

Satellite	Azimuth
GOES-8	145.2°

The next table gives the coordinates for the four corners of the flight path, ignoring the allowance for turning shown in the figure above

Flight Path Definitions

Corner	*UTM*			*Lat*	*Long*
S	632735	4038289	14	36°28.8'N	97°31.1'W
E	648959	4049985	14	36°35.0'N	97°20.1'W
N	637263	4066209	14	36°43.9'N	97°27.8'W
W	621039	4054513	14	36°37.7'N	97°38.8'W

Special Needs

The MPIR must be mounted on the UAV to view downward from 51° to -29° favoring the port side instead of its normal ±40° nadir mount for the Fall 1996.

Instrument and Data List

UAV

Instrument 1: MPIR four channels (0.62-0.67 μm, 0.86-0.90 μm, 1.36-1.39 μm, and 1.58-1.64 μm) each yielding data from a 256 element linear array (512 element for band 1) that is oriented to provide a curved, across track radiometric line image; the line images are spatially co-registered and temporally sampled each 0.5 second (0.25 for band 1); the instantaneous FOV for each pixel is 6 mrad (3 mrad for band 1)

Instrument 2: CDL 200 range bins with intensity of reflected laser light plus one background bin; range bins provide information on the location and density of aerosols/clouds; background bin for data correction

Instrument 3: zenith TDDR downwelling hemispherical flux data; seven channels each 10 nm wide; channel center wavelengths are 0.5, 0.86, 1.0, 1.25, 1.5, 1.65, and 1.75 μm; shadow rings move across the FOV periodically blocking direct solar radiation thus enabling determination of the diffuse : direct ratio

Instrument 4: zenith IRBBR broadband radiometer with hemispherical FOV; measures downwelling flux from 4 to 30 μm

Instrument 5: nadir IRBBR broadband radiometer with hemispherical FOV; measures upwelling flux from 4 to 30 μm

Instrument 6: zenith SBBR broadband radiometer with hemispherical FOV; measures downwelling flux from 0.3 to 4 μm

Instrument 7: nadir SBBR broadband radiometer with hemispherical FOV; measures upwelling flux from 0.3 to 4 μm

Instrument 8: nadir SSP2 reflected spectral radiance in $Wm^{-2}sr^{-1}nm^{-1}$, 0.4 to 4.0 μm; reflected spectral flux in $Wm^{-2}nm^{-1}$, 0.4 to 2.5 μm; 2 channels linearly polarized ($||$, $\perp$) reflected spectral radiance in $Wm^{-2}sr^{-1}nm^{-1}$, 0.4 to 2.5 μm; reflected broadband radiance in $Wm^{-2}sr^{-1}$, 0.4 to 4.0 μm; reflected broadband flux in Wm^{-2}, 0.4 to 2.5 μm

Ground

Instrument 1: MMCR (all variants) zenith-pointing radar that operates at a frequency of 35 GHz to determine cloud boundaries (e.g., cloud bottoms and tops) and radar reflectivity (dBZ) of the atmosphere up to 20 km; has a Doppler capability that will allow the measurement of cloud constituent vertical velocities

Instrument 2: MWR water vapor density profile and five-minute averages of column integrated water vapor, column integrated liquid water, and blackbody equivalent brightness temperature

Instrument 3: zenith IRT ground-based radiation pyrometer that provides measurements of the equivalent black body brightness temperature of the scene in its field of view; has a narrow field of view for measuring the temperature of the sky or cloud base

Instrument 4: WSI image of entire sky dome; 0.33° angular resolution; 16 bit dynamic range; image grab every 10 sec; day time image is red filtered (650 nm) and blue filtered (450 nm); night time image not filtered; derived products include calibrated radiance map of sky dome, cloud cover fraction, and segmented image into opaque clouds, thin clouds, and clear

Instrument 5: Raman lidar 355 nm laser system providing profiles of water vapor, aerosols, and optically thin clouds with 40 meter resolution; maximum altitude for water vapor is 4 km daytime and 10 km night time; maximum altitude for aerosols and clouds is 15 km

Instrument 6: radiosonde balloon borne instrument measuring temperature, pressure, water vapor, and winds from its surface launch point upwards to a 35 km altitude during a 2 hour period

Instrument 7: 915 MHz profiler with RASS profiles of virtual temperature, wind speed, and wind direction

Instrument 8: 50 MHz profiler with RASS profiles of virtual temperature, wind speed, and wind direction

Instrument 9: Lamont SIRS direct beam normal solar irradiance; downwelling diffuse solar irradiance; downwelling hemispherical solar irradiance; upwelling hemispherical solar irradiance; downwelling hemispherical infrared radiance

Instrument 10: Lamont MFRSR hemispheric downward solar irradiance (415, 500, 610, 665, 862, and 940 nm); hemispherical downward total solar irradiance; diffuse hemispherical downward solar irradiance (415, 500, 610, 665, 862, and 940 nm) diffuse hemispherical downward total solar irradiance; direct beam normal solar irradiance (415, 500, 610, 665, 862, and 940 nm); and direct beam normal total solar irradiance

Instrument 11: AERI two data for wave numbers between 520 and 1800 cm^{-1}: mean infrared radiance spectral ensemble and the standard deviation for that ensemble; three data for the six bands of 675-680, 700-705, 985-990, 2295-2300, 2282-2287, 2510-2515 cm^{-1}: mean radiance, standard deviation of that radiance, and brightness temperature

Satellite GOES-8:

Instrument 1: imager (visible) multi-channel instrument designed to sense radiant and solar-reflected energy from sampled areas of the Earth; produces full-Earth disc images with 1 km resolution

Instrument 2: imager (infrared) multi-channel instrument designed to sense radiant and solar-reflected energy from sampled areas of the Earth; produces full-Earth disc images with 4-km resolution

Satellite GOES-9:

Instrument 1: imager (visible) multi-channel instrument designed to sense radiant and solar-reflected energy from sampled areas of the Earth; produces full-Earth disc images with 1 km resolution

Instrument 2: imager (infrared) multi-channel instrument designed to sense radiant and solar-reflected energy from sampled areas of the Earth; produces full-Earth disc images with 4-km resolution

Satellite NOAA-12:

Instrument 1: AVHRR cross-track scanning system with five spectral channels; the spectral band widths are 0.58-0.68, 0.725-1.10, 3.55-3.93, 10.3-11.3, and 11.5-12.5 μm; IFOV of each channel is approximately 1.4 mrad leading to a resolution at the satellite sub-point of 1.1 km for a nominal altitude of 833 km; IR channels are calibrated in-flight; no in-flight visible channel calibration is performed

Satellite NOAA-14:

Instrument 1: AVHRR cross-track scanning system with five spectral channels; the spectral band widths are 0.58-0.68, 0.725-1.10, 3.55-3.93, 10.3-11.3, and 11.5-12.5 μm; IFOV of each channel is approximately 1.4 mrad leading to a resolution at the satellite sub-point of 1.1 km for a nominal altitude of 833 km; IR channels are calibrated in-flight; no in-flight visible channel calibration is performed

Appendix A: Contact List

Will Bolton, Sandia National Laboratories, Mail Stop 9104, Livermore, California 94551-0969; phone: 510-294-2203; fax: 510-294-1377; email: wrbolton@sandia.gov

Roger Busbee, Sandia National Laboratories, Mail Stop 9101, Livermore, California 94551-0969; phone: 510-294-2147; fax: 510-294-1539; email: rlbusbe@ca.sandia.gov

Robert Cahalan, Senior Research Scientist, NASA / GSFC, Code 913, Greenbelt, Maryland 20771; phone: 301-286-4276; fax: 301-286-1627; email: cahalan@clouds.gsfc.nasa.gov

Ric Cederwall, Atmospheric Science Division (L-103), Lawrence Livermore National Laboratory, P.O. Box 808, Livermore, California 94551; phone: 510-422-6831; fax: 510-423-4908; email: rcederwall@llnl.gov

Thomas Charlock, Mail Stop 420, NASA / Langley, Hampton, Virginia 23681-0001; phone: 804-864-5687; fax: 804-864-7996; email: t.p.charlock@larc.nasa.gov

Richard Coulter, Building 203, Environmental Research Division, Argonne National Laboratory, 9700 S. Cass Ave., Argonne, Illinois 60439; phone: 708-252-5833

Patrick Crowley, Environmental Science Division, ER-74, U.S. Department of Energy, Washington, DC 20585; phone: 301-903-3069; fax: 301-903-8519; email: crowley@oerhp01.doe.gov

Peter Daum, Chemist, Environmental Chemistry Division, Brookhaven National Laboratory, Upton, New York 11973-5000; phone: 516-344-7283; fax: 516-344-2887; email: phdaum@bnlux1.bnl.gov

Robert Ellingson, Department of Meteorology, University of Maryland, College Park, Maryland 20742; phone: 301-405-5386; fax: 301-314-9482; email: bobe@atmos.umd.edu

Michael Ferrario, Sandia National Laboratories, Mail Stop 9014, Livermore, California 94551-0969; phone 510-294-2827; fax 510-294-1015; email: mike_ferrario@sandia.gov

Weigang Gao, Building 203, Environmental Research Division, Argonne National Laboratory, 9700 S. Cass Ave., Argonne, Illinois 60439; phone: 630-252-4008; fax: 630-252-5498

Catherine Gautier, Professor of Geography, University of California, Computer Systems Laboratory, Santa Barbara, California 93106; phone: 805-893-4885; fax: 805-893-2578; email: gautier@icess.ucsb.edu

Susan Havre, Pacific Northwest Laboratories, P.O. Box 999, K7-28, Richland, Washington 99352; phone: 509-375-6948; fax: 509-375-3641; email: sl_havre@arm.gov

Peter LaDelfe, Los Alamos National Laboratory, NIS-2, MS-D436, Los Alamos, New Mexico 87545; phone: 505-667-1597; fax: 505-667-3815; email: pladelfe@lanl.gov

Arno Ledebuhr, Lawrence Livermore National Laboratory, P.O. Box 808, MS L0285, Livermore, California 94550; phone: 510-423-1184; fax: 510-423-1243; email: ledebulr1@llnl.gov

Bob McCoy, Colorado State University, Atmospheric Science Department, Fort Collins, Colorado 80523; phone: 970-491-8038; fax: 970-491-8449; email: mccoy@herschel.atmos.colostate.edu; web: http://optical.atmos.colostate.edu

Kuo-Nan Liou, Professor and Director / CARSS, Department of Meteorology, Room 819 W.B.B., University of Utah, Salt Lake City, Utah 84112; phone: 581-3336; fax: 801-581-4065; email: knliou@climate.utah.edu

Patrick Minnis, NASA Langley Research Center, Mail Stop 420, Hamption, Virginia 23681-0001; phone: 804-864-5671; fax: 804-864-7996; email:: p.minnis@larc.nasa.gov

Gary Phipps, Sandia National Laboratories, Mail Stop 0980, Albuquerque, New Mexico 87185-0980; phone 505-845-8269; fax 505-844-2057; email: gsphipp@sandia.gov

Shelly Pope, Atmospheric Research Laboratory, Scripps Institute of Oceanography, University of California, San Diego, California; phone: 619-534-9619; fax: 619-534-7452; email: pope@arlo.ucsd.edu

Paul Racette, Microwave Sensor Branch, Code 975, NASA, Goddard Space Flight Center, Greenbelt, Maryland 20771; phone: 301-286-9114; fax: 301-286-0294; email: per@meneg.gsfc.nasa.gov

Henry Revercomb, The Cooperative Institute for Meteorological Satellite Studies, Space Science and Engineering Center at the University of Wisconsin-Madison, 1225 West Dayton Street, Madison, Wisconsin 53706; phone: 608-263-6758; fax: 608-262-5974; email: hankr@ssec.wisc.edu

Dan Rodriguez; Lawrence Livermore National Laboratory, P.O. Box 808, Livermore, California 94551 phone: 510-422-1833; fax: 510-423-4908; email: rodriguez5@llnl.gov

Stephen Schwartz, Senior Chemist, Environmental Chemistry Division, Brookhaven National Laboratory, Upton, New York 11973; phone: 516-344-3100; fax: 516-344-2887; ses@bnl.gov

William Smith, The Cooperative Institute for Meteorological Satellite Studies, Space Science and Engineering Center at the University of Wisconsin-Madison, 1225 West Dayton Street, Madison, Wisconsin 53706; phone: 608-262-0544

Dave Sowle, Mission Research Corporation, 735 State Street, P.O. Drawer 719, Santa Barbara, California, 93102; phone: 805-963-8761, x245; fax: 805-962-8530; email: sowle@mrcsb.com

Graeme L. Stephens, Colorado State University, Department of Atmospheric Science, Ft. Collins, Colorado 80523-1371; phone: 970-491-8550; fax: 970-491-8449; email: stephens@langley.atmos.colostate.edu

Tim Tooman, Sandia National Laboratories, MS 9056, Livermore, California 94551-0969; phone: 510-294-2752; fax: 510-294-1377; email: tooman@ca.sandia.gov

Francisco Valero, California Space Institute, Scripps Institution of Oceanography, University of California, San Diego, California

92093-0230; phone: 619-534-6382; fax: 415-604-3625; email: francisco_valero@qmgate.arc.nasa.gov

John Vitko, Jr., Sandia National Laboratories, MS 9056, Livermore, California 94551-0969; phone: 510-294-2820; fax: 510-294-2276; email: john_vitko@sandia.gov

Paul Weber, Los Alamos National Laboratory, NIS-2, D436, Los Alamos, New Mexico 87545; phone: 505-667-5776; fax: 505-667-3815; email: pweber@lanl.gov

James Weinman, Microwave Sensor Branch, Code 975, NASA, Goddard Space Flight Center, Greenbelt, Maryland 20771; phone: 301-286-3175; fax: 301-286-0294; email: weinman@sensor.gsfc.nasa.gov

Appendix B: Acronym and Symbol List

ADM	anisotropic directional models
AERI	atmospherically emitted radiation interferometer
AMMR	Airborne Multichannel Microwave Radiometer
ARESE	ARM Enhanced Shortwave Experiment
ARM	Atmospheric Radiation Measurement (program)
AVHRR	advanced very high resolution radiometer
CART	Cloud And Radiation Testbed
CDL	cloud detection lidar
CERES	cloud and earth radiant energy system
CSR	clear-sky reflectance
D	cloud effective particle diameter
DAM	directional albedo model
DD	cloud effective water droplet diameter
ER-2	extended range U-2 aircraft
FOV	field of view
FSBBR	fractional solar broadband radiometer
GOES	geostationary operational environmental satellite
GRAMS	ground-based radiation measurement system
HONER	hemispherical optimized net radiometer
ID	cloud effective ice crystal diameter
IFOV	instantaneous field of view

IRBBR	infrared broadband radiometer
IW	cloud ice water path
LIDAR	light detection and ranging
LLNL	Lawrence Livermore National Laboratory
LW	cloud liquid water path
MFRSR	multifilter rotating shadowband radiometer
MWR	millimeter-wave radiometer
MMCR	millimeter-wave cloud radar
MPIR	multispectral pushbroom imaging radiometer
MSL	mean sea level
MWR	microwave radiometer
NASA	National Aeronautics and Space Administration
NOAA	National Oceanographic and Atmospheric Administration
RAMS	radiation measurement system
RASS	radio acoustic sounding system
SBBR	solar broadband radiometer
SGP	southern great plains
SIRS	spectrally integrated radiometers
SMOS	surface meteorological observation system
SPFR	solar spectral flux radiometer
SPS	spatial power spectrum
SSP	spectrally scanning polarimeter
SZA	solar zenith angle
TDDR	total direct diffuse radiometer

TOA	top of atmosphere
T_s	surface skin temperature
UAV	unmanned aerospace vehicle
VZA	viewing zenith angle
W	cloud water path, either ice or water
WSI	whole sky imager

Appendix C: References

[1] Robert Ellingson and Tim Tooman, eds., ARM UAV Science and Experiment Plan, 1996 Flight Series, Revision 4, March 2, 1996.

[2] Francisco P. J. Valero, et. al., ARESE (ARM Enhanced Shortwave Experiment) Science Plan .